Engineering Structures 353 (2026) 122347

Contents lists available at ScienceDirect

Engineering Structures

journal homepage: www.elsevier.com/locate/engstruct

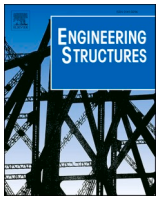

From code to performance: Probabilistic seismic response of retrofitted precast RC buildings

Luca Capacci [a], Chiara Di Salvatore [b], Marius Eteme Minkada [c], Davide Bellotti [d], Francesco Cavalieri [d], Bruno Dal Lago [e], Gennaro Magliulo [f], Paolo Riva [c], Andrea Belleri [c,*]

[a] Politecnico di Milano, Department of Civil and Environmental Engineering, Milan, Italy
[b] Università di Napoli Parthenope, Department of Science and Technology, Napoli, Italy
[c] Università degli Studi di Bergamo, Department of Engineering and Applied Sciences, Bergamo, Italy
[d] European Centre for Training and Research in Earthquake Engineering, Pavia, Italy
[e] Università degli Studi dell'Insubria, Department of Theoretical and Applied Sciences, Varese, Italy
[f] Università degli Studi di Napoli Federico II, Department of Structures for Engineering and Architecture, Napoli, Italy

ARTICLE INFO

Keywords:
Industrial buildings
Precast concrete
Seismic retrofit
Code-based design
Performance-based assessment
Probabilistic analysis
Fragility curves
Seismic risk

ABSTRACT

Inadequate detailing in precast buildings designed under previous codes has proven to be a key factor in the seismic vulnerability of Italy's industrial heritage. Advances in structural assessment and refined hazard mapping have led to strategies now embedded in design guidelines; however, their actual probabilistic performance remains an open issue. This paper investigates the probabilistic seismic vulnerability of four single-story precast RC buildings constructed between the 1960s and 1990s, each emblematic of its decade, in a high seismic hazard area designed according to the codes of the time and retrofitted according to the current Italian code. A rigorous validation of standard code-compliant retrofit strategies is proposed, using a fully probabilistic framework that incorporates non-linear pushover analysis, multi-stripe analyses, and fragility derivation methods, which are typically not used in practical code-based design verification. For each case, the effectiveness of the designed retrofit measures is assessed through advanced analyses at two performance levels: usability preventing damage (UPD) and global collapse (GC). Results show that highly invasive global retrofit solutions achieve safety targets consistent with current code requirements for Global Collapse. Furthermore, all proposed interventions substantially reduce the mean annual failure rate for the UPD limit state, keeping retrofitted archetypes within safety margins. Overall, the study provides a concise quantitative benchmark for assessing the effectiveness of current retrofit standards for precast industrial buildings on a probabilistic basis, tailored to specific typologies from different decades.

1. Introduction

Precast industrial buildings in Southern Europe, designed according to older codes, are often characterised by critically poor detailing and, consequently, inadequate structural performance. This is mainly due to limited prior knowledge of seismic hazard and design, as observed in post-earthquake surveys [1–5]. Advanced analyses of the seismic behaviour of existing industrial precast buildings have confirmed these issues, although they refer to very different structural typologies of precast industrial structures, each with specific problems arising from their historical evolution [6–10]. This pronounced seismic vulnerability has highlighted the major challenge of optimally retrofitting the existing industrial building stock [11]. In this context, several retrofit interventions have been investigated, including innovative solutions such as the installation of dissipative devices in beam-to-column joints, both rotational [12–15] and translational [16,17], the insertion of dampers within stiffening braces [15,18,19], between the flexible frame structure and the stiffer cladding panels [20], or at the base of columns [21]. However, the aforementioned studies address the efficiency of individual retrofitting techniques and do not provide information on their combined use, which is typically required to significantly improve the seismic performance of precast industrial buildings. Furthermore, the

* Corresponding author.
E-mail address: andrea.belleri@unibg.it (A. Belleri).

https://doi.org/10.1016/j.engstruct.2026.122347
Received 16 August 2025; Received in revised form 20 December 2025; Accepted 9 February 2026
Available online 18 February 2026

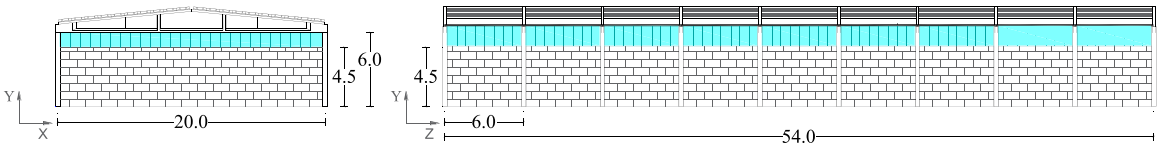

Fig. 1. Building EE1 – frontal and side view. (Units: m).

wide variety of precast industrial building typologies means that some techniques are only suitable or applicable to a limited portion of the existing stock. As a result, there is currently a lack of probabilistic data necessary for risk analyses regarding the efficiency of retrofitting interventions for large stocks of precast industrial buildings, which hinders the planning activities of governmental bodies.

To provide an additional, up-to-date contribution to this critical field, this paper presents part of the results obtained within the ReLUIS project 2022/2024, funded by the Italian Department of Civil Protection. The project addresses the evaluation of the effectiveness of retrofitting measures on existing structures designed according to previous Italian building codes from the 1960s to the 1990s. Previous research within the RINTC-Implicit Seismic Risk of Code-conforming Structures project, part of the ReLUIS programme, focused on assessing the probabilistic seismic vulnerability of single-storey precast industrial RC buildings designed according to the current Italian building code [22–26] or previous codes from the 1960s to the 1990s [27–30]. This work builds on a previous study of the seismic risk of as-built precast buildings [31] by investigating the effectiveness of retrofitting strategies on the same case studies. The methodology adopted in the RiNTC framework has also inspired seismic fragility assessments of several structural typologies, including residential buildings [32–36], bridges and overpasses [37], industrial steel structures [38], and benchmarking of real buildings in recent earthquakes [39]. This work examines four precast RC single-storey existing industrial buildings and aims to bridge the gap between (a) simulated code-based seismic retrofit design and (b) performance-based, fully probabilistic seismic fragility and risk assessment. While most recent studies either investigate innovative retrofit techniques on new and existing structures or develop comprehensive performance-based assessments on single case studies, this study offers a systematic evaluation of traditional retrofit techniques applied to a range of archetypes broad enough to represent most precast RC structural assemblies constructed in Italy between the 1960s and 1990s.

The selection of benchmark buildings is based on key structural features such as geometry, original design code, connection layout, peripheral cladding, and diaphragm configuration. Retrofit strategies are developed according to the simplified numerical procedures allowed by the current Italian design code for existing buildings. The Performance-Based Earthquake Engineering (PBEE) framework is then used to explicitly quantify the improvement in seismic risk mitigation provided by the designed interventions. Statistical fitting methods are subsequently employed to estimate seismic fragility curves and annual failure rates for both as-is and retrofitted buildings, using non-linear numerical modelling and structural analysis tools, such as nonlinear static and multi-stripe time-history dynamic analyses. This dual approach enables a consistent evaluation of the effectiveness of conventional code-compliant retrofit solutions under record-to-record variability and multiple failure modes (UPD and GC), and highlights the influence of connection detailing, cladding-to-structure interaction, and diaphragm behaviour on retrofit efficiency. Section 2 briefly reviews established but relevant insights on current code-based seismic assessment in Italy. Section 3 describes the geometric features and construction details of each case study building and presents the results of the code-based seismic assessment. Section 4 proposes code-compliant retrofit strategies tailored to each building and thoroughly discusses practical implications for their design and implementation. Section 5 presents a detailed modelling strategy for advanced seismic assessment using nonlinear static pushover analysis and nonlinear time-history Multi-Stripe Analysis (MSA). Section 6 addresses risk estimates for fragility curves and failure rates, providing comparisons and comments on the previous results of the as-built assessment of the non-retrofitted structures in terms of two performance levels: Usability Preventing Damage (UPD) and Global Collapse (GC).

2. Highlights on code-conforming seismic assessment and retrofit design

The Italian standard NTC 2018 [40,41] formally establishes general criteria for the safety assessment of existing structures, as well as for the design, execution, and proof-load testing of retrofitting measures to improve structural and seismic performance. In particular, the safety assessment and design of interventions should consider the state of knowledge at the time of construction, including the possible detection of design and construction flaws, signs of damage caused by serviceability or exceptional actions, and significant deterioration compared to the original condition. Structural models are then created based on the level of detail in the available historical documentation and the results of on-site investigations regarding geometry and detailing, mechanical properties of materials and soils, and permanent loading conditions.

Despite the tools available in the Italian standard for seismic retrofit design, the current code does not provide uniform risk-based methods as presented in this paper. To realistically simulate the design process, the retrofit measures in the case study are designed according to the guidelines of the Italian code for modelling structural systems and seismic actions, as well as the analysis tools for seismic demand assessment. Structural models should be three-dimensional and should adequately represent the actual spatial distribution of mass, stiffness, and resistance. Seismic actions are usually site-specific response spectra and limit states adapted to the ductility class of the building. Equivalent static forces or correspondingly selected ground motion time histories are used less frequently. The assessment of seismic demand is generally performed using linear analysis methods, although special limitations apply to geometric nonlinearities that depend on the drift capacity of vertical structural elements. A seismic demand assessment that includes mechanical nonlinearities is also permitted and can be adopted by the designer to better represent the available dissipative resources of the components, especially when seismic protection devices are used.

In the following subsections, each building is briefly described by its structural typology and construction period. The results of the seismic assessment are then discussed using a code-based as-built approach, highlighting structural deficiencies based on insufficient safety indices, ζ_E in relation to NTC 2018 standards [40,41].

3. Case study buildings

The most important geometric features of the case study buildings have already been presented in Bosio et al. [31]. In this paper, the same naming convention (EE1, EE2, EE3, EE4) as in the previous study is maintained. The following sections summarise the main historical and geometric characteristics of the studied buildings, all located in L'Aquila on Type C soils according to the Eurocode 8 classification (EN 1998-1:2004 [42]).

Building EE1 (Fig. 1) reflects the design criteria of the late 1960s and early 1970s in L'Aquila. It has a rectangular floor plan measuring 20 × 54 m^2, with ten single-span portal frames. The 6 m high square columns are set into concrete-filled socket foundations. The main beams,

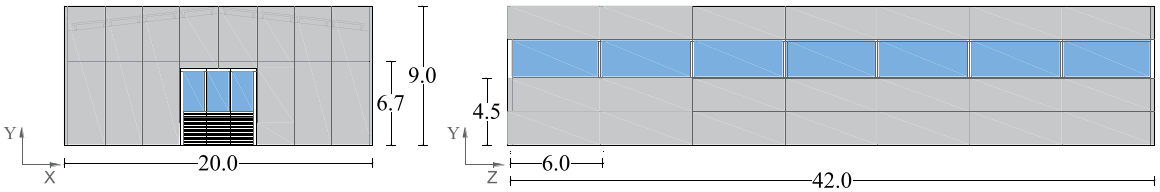

Fig. 2. Building EE2 – frontal and side view. (Units: m).

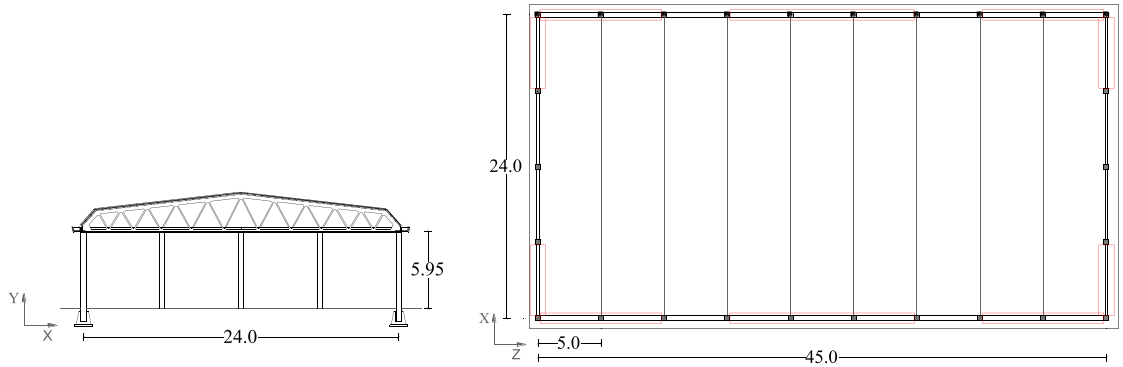

Fig. 3. Building EE3 – frontal view and plan view with infill walls arrangement. (Units: m).

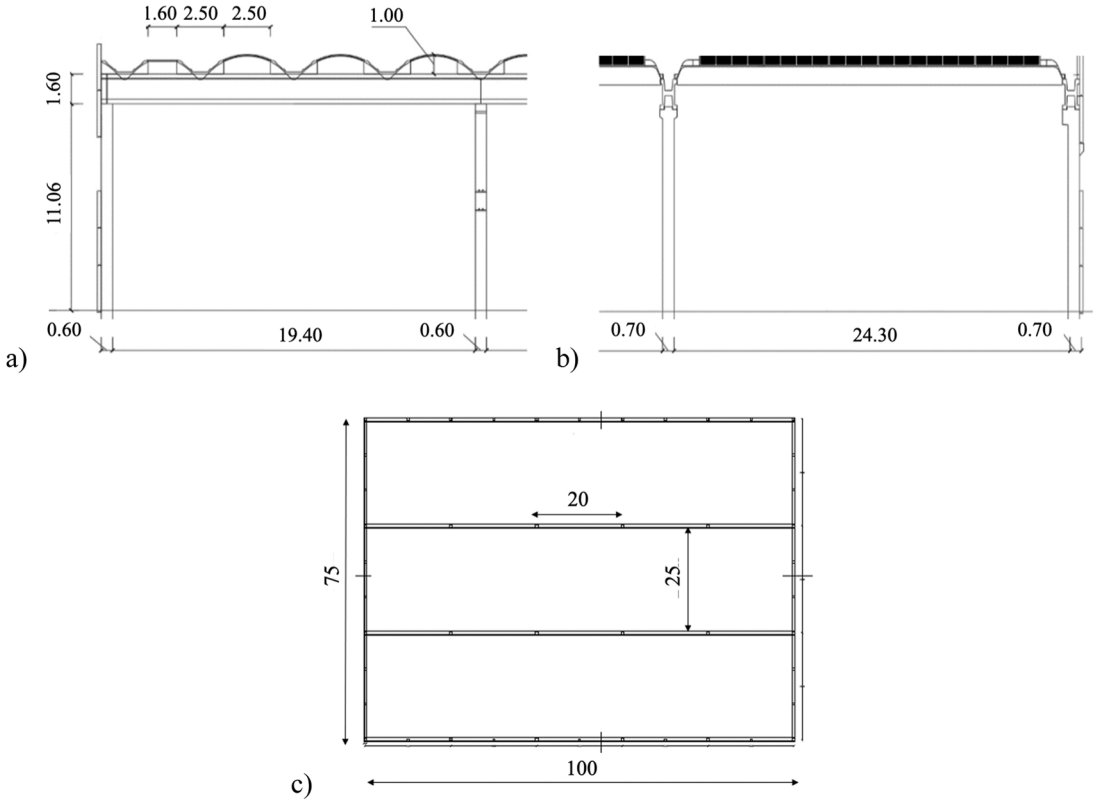

Fig. 4. Building EE4 – (a) section view parallel to the wing-shaped roof elements (transverse direction), (b) section view parallel to the H-beams (longitudinal direction), and (c) plan view. (Units: m).

with a 10 % inclined double slope and a 20 m span, have a T-section at the ends and an I-section with varying heights and thicknesses along the entire span. The connections between the columns and beams include small-diameter (ϕ 10 mm) steel dowels. The roof consists of prestressed double-T elements rigidly connected to the main beams. The outer walls are brickwork with 1.5 m high ribbon windows.

Building EE2 (Fig. 2) dates from the second half of the 1980s and has a floor plan of 20 × 42 m^2 with a clear height of 7 m beneath the beams. The structural frame consists of 16 precast columns arranged in a regular 6 × 20 m^2 grid. The double-tapered main beams are connected to the columns by reinforced concrete forks, with friction connections along the X-axis, whereas the secondary roof elements are double-tee beams.

Table 1
Synoptic table for the case study structural features.

Building	EE1	EE2	EE3	EE4
Construction period	1960–1970s	1980s	1970s	1990–2000s
Reference design code	CNR-UNI 10012/1967 [44] D.M. 30/05/1974 [45] D.M. 03/03/1975 [46]	D.M. 19/06/1984 [47] CNR-10025/1984 [48]	CNR-UNI 10012/1967 [44] D.M. 30/05/1974 [45] D.M. 0303/1975 [46]	D.M. 09/01/1996 [49]
Structural features	Roof concrete topping Infill masonry cladding Weak dowel connections	Flexible diaphragm External panels Weak dowel connections	Roof concrete topping Infill masonry cladding Friction connections	Flexible diaphragm External panels Panel-bearing columns Weak slab dowels Relevant P-Delta effect

The closure consists of precast reinforced concrete panels, with ribbon windows placed between the third and fourth horizontal panel rows.

Building EE3 (Fig. 3) is inspired by an industrial building erected in Naples in 1973 and has been redesigned for the case of L'Aquila. It features a rectangular floor plan measuring 45 × 24 m^2, with ten RC trusses spanning the transverse direction. Prefabricated square columns divide the short side into four bays, each 6 m long. Independent socket foundations support the columns. Along the Z-axis, there are nine spans of 5 m each, supporting secondary beams shaped to allow water drainage. The roof comprises pre-stressed double-tee panels attached to the main beams with a 5 cm-thick composite deck. The outer walls are symmetrically distributed along the perimeter (red spans in Fig. 3) and consist of 25 cm-thick unreinforced masonry. Principal beams are simply supported on column heads through the interposition of a single layer of neoprene pad.

Building EE4 (Fig. 4) was built in the late 1990s and represents a modern, large-span precast industrial building with five bays and three naves. The main frames along the Z-axis comprise 11 m-high columns and H-beams, while the roof consists of wing-shaped elements [43] with vaulted or shed closures. The horizontal cladding panels extend around the entire perimeter, with window bands located between the upper and lower panels. Additional supporting columns, structurally independent of the main frames, support the horizontal panels.

Table 1 summarises the main characteristics of each case study in terms of construction time, the Italian code used as a reference for the simulated design that defines the as-built condition, and the relevant highlights of the structural typologies studied.

The selected case-study buildings are intended to represent a broad range of single-storey precast industrial structures commonly found in Southern Europe [50], spanning different construction decades, structural layouts, connection details, and diaphragm configurations, all of which are known to significantly influence seismic performance. Although other typologies, such as multi-bay buildings with irregular layouts or structures designed according to post-2000 Italian codes, are not explicitly considered, the chosen cases capture the most recurrent characteristics of the existing building stock.

4. Code-based seismic assessment and retrofit design

The seismic capacity of existing buildings is assessed by comparing it with the requirements for new buildings using the safety index ζ_E. This index is defined as the ratio of the actual seismic intensity, typically expressed as peak ground acceleration (PGA), that a structure can withstand for a given limit state, to the seismic design action specified for new, code-compliant buildings on the same site. As-built structural safety is evaluated with respect to the Life Safety Limit State, considering a seismic reference intensity corresponding to a PGA with a return period of $T_n = 475$ years. In this study, the safety index ζ_E. is calculated for each type of potentially vulnerable structural element and connection, as typically done by a professional engineer. The ζ_E. values are determined through response spectrum analysis, assuming a behaviour factor of 1.5 (non-dissipative). Three-dimensional elastic models are developed using Midas Gen [51] for EE1 and EE2, SAP2000 [52] for EE3, and Straus7 [48] for EE4. A full state of knowledge is assumed for all buildings, resulting in unit confidence factors for the mechanical properties of the materials. For the structural capacity assessment, the flexural and shear resistances are evaluated based on code-compliant approaches, while the connection strengths depend on the structural typologies investigated. Finally, the conceptual design for the adopted retrofit strategies is presented, and a code-compliant evaluation is performed to numerically validate the proposed solutions.

Table 2
Safety levels ζ_E for each building and investigated failure mode (values lower than 1.00 in bold).

Building	EE1	EE2	EE3	EE4
Beam-to-column connection	**0.06**	1.04	**0.02**	**0.63**
Roof-to-beam connection	>>1	**0.92**	>>1	**0.16**
Masonry cladding strut	1.56	-	1.42	-
Panel-to-column connection	-	**0.16**	-	**~ 0.00**
Column (bending)	**0.36**	**0.53**	4.87	**0.62**
Column (shear)	**0.20**	1.10	2.10	> >1

In building EE1, dowel-based connections are modelled as pinned connections, and the potential occurrence of joint sliding is checked *a posteriori* based on the analysis results. The safety index (ζ_E) is assessed for columns and beam-to-column connections. Column evaluation covers both shear and bending mechanisms. The collapse mechanism related to roof-to-beam connections is disregarded, as roof elements are rigidly fastened to the main beams. The minimum value is attained along the y-direction for dowel failure (i.e. $\zeta_E = 0.06$), mainly due to the small dowel diameter (ϕ 10 mm). The shear resistance of the dowel is evaluated using the formulation proposed by CNR 10025/1984 [48], as the Italian code does not provide guidance in this respect.

For building EE2, the safety level in as-built conditions is evaluated with reference to the columns, as well as the roof-to-beam, horizontal panel-to-column, and vertical panel-to-beam connections. Regarding the collapse mechanism, the same considerations apply as for building EE1. Widespread deficiencies are found in the connections between cladding panels and the main structural element, with ζ_E equal to 0.16 and 0.41 for vertical and horizontal panels, respectively. Further deficiencies are observed in the connections between the roof element and the beams, as well as in the columns (for bending), with ζ_E equal to 0.92 and 0.53, respectively.

For building EE3, the safety indices ζ_E are evaluated for the columns, beam-to-column connections, and infill walls. The frictional connections between neoprene and concrete are checked based on the resulting horizontal forces, using Coulomb friction with a coefficient calibrated according to Magliulo et al. [53]. The infill shear strength is assessed using the method proposed by Decanini et al. [54], considering the maximum strength of the infill wall under four possible failure modes: diagonal tension, sliding shear along the horizontal joints, crushing in the corners in contact with the frame, and diagonal compression. The only structural deficiency identified is in the friction joints, which exhibit very low values of the safety index ζ_E.

The seismic assessment of building EE4 included columns, beam-to-column connections, roof-to-beam connections, and panel-to-structure

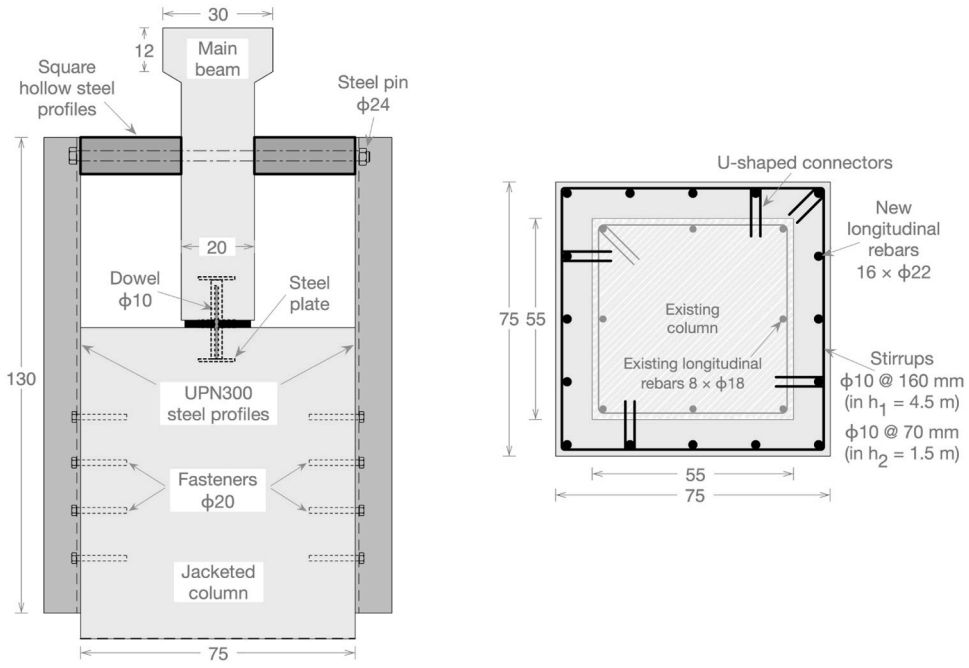

Fig. 5. Building EE1 – elevation and cross section of concrete jacketing. (Units in cm, unless otherwise specified).

connections. Columns and beam-to-column connections have a vulnerability index ζ_E of just over 0.60, while the vulnerabilities associated with the roof-to-beam and panel-to-structure connections are significantly higher. For the panel-to-structure connections, it is assumed that the use of fixed strap connections with very limited in-plane displacement capacity results in complete vulnerability. This is due to their incorrect design, which does not allow structural decoupling between the panel and the structure and neglects in-plane seismic actions [55].

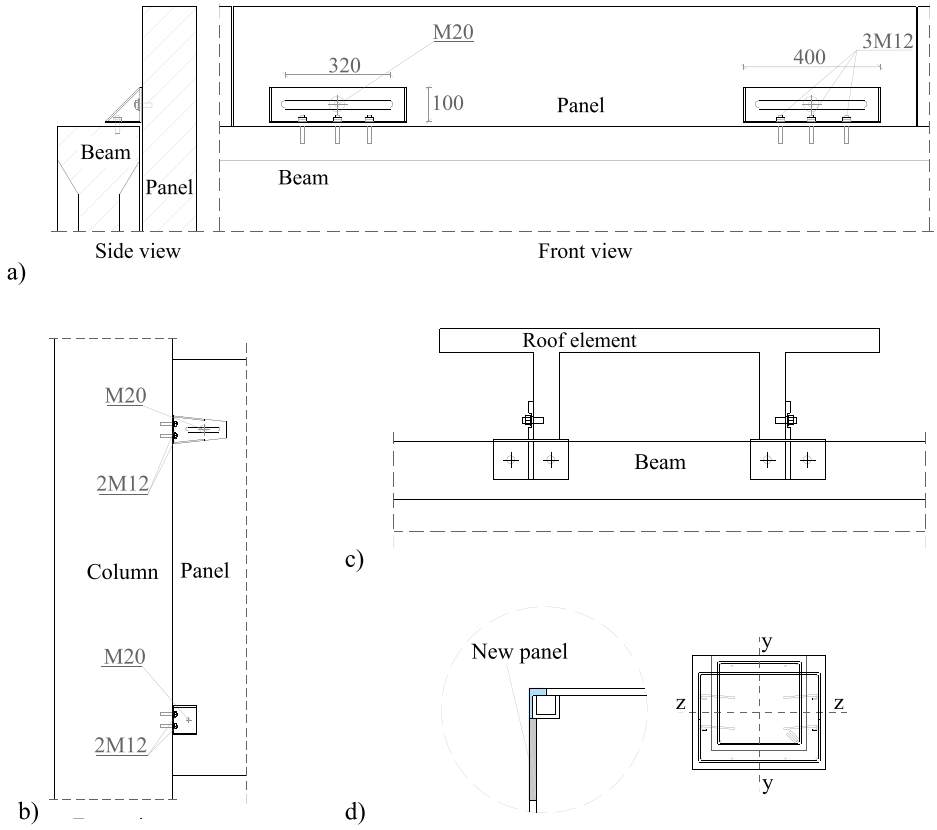

Fig. 6. Building EE2 – schematic details of (a) vertical panel-to-column connection, (b) horizontal panel-to-column connection, (c) roof-to-beam connection, (d) column jacketing scheme and vertical end panel replacement. Note: The reported dimensions are in mm; S275 steel and 8.8 grade bolts were adopted.

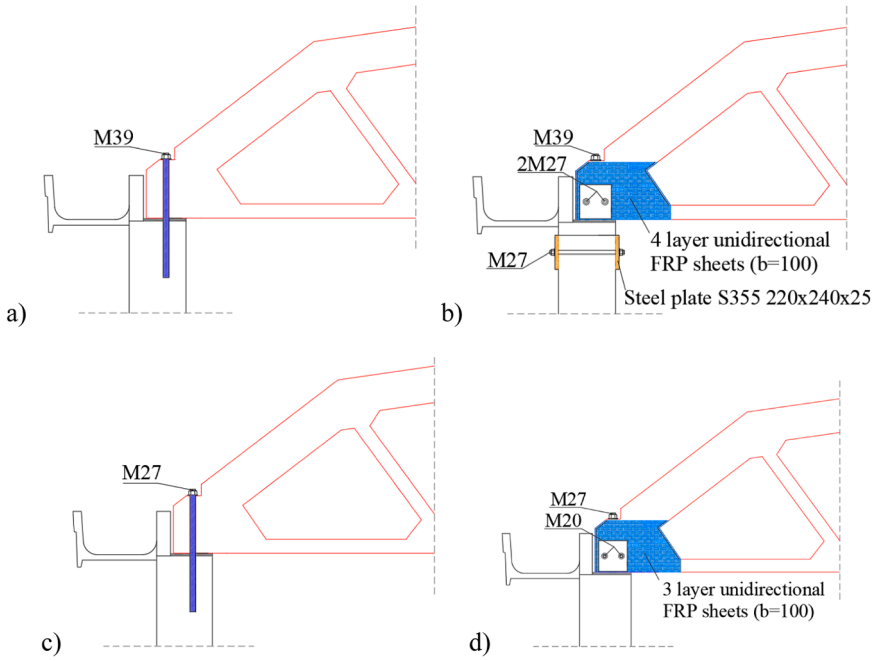

Fig. 7. Building EE3 – design of beam-to-column connections: (a,b) corner columns, (c,d) lateral columns. Note: The reported dimensions are in mm; 10.9 grade dowels were adopted.

Table 2 presents the minimum values of the safety indices for all collapse mechanisms investigated. All scenarios examined result in high seismic vulnerability.

4.1. Design of seismic retrofit interventions

The Italian standard classifies interventions on existing buildings into three categories: (1) repairs or local interventions affecting individual structural elements without significantly altering overall structural performance; (2) improvement interventions that increase pre-existing structural safety without necessarily achieving the safety levels required for new buildings; and (3) full code-conforming interventions that aim to increase structural safety to meet the standards required for new buildings. The case studies presented in this paper examine various retrofit measures that ultimately upgrade the buildings analysed. In these cases, the retrofitting provides full code compliance to ensure a safety index of $\zeta_E \geq 1.0$.

4.1.1. Building EE1

The retrofit measure, which involves RC jacketing of the columns and local beam-to-column joint strengthening with steel profiles, is shown in Fig. 5. Concrete class R_{bk} 350 [kg/cm^2] is assigned to the columns from the 1970s. The jacketing of the columns is designed with C28/35 class concrete, in accordance with current Italian seismic regulations, which recommend a limited difference in concrete class between new and existing material. Sixteen ϕ 22 mm longitudinal reinforcement bars in B450C grade steel are designed following a linear dynamic analysis with the model used in the assessment. The resulting 1 % reinforcement ratio also corresponds to the minimum ratio prescribed by NTC 2018 [40,41]. The transverse reinforcement consists of ϕ 10 mm stirrups with a spacing of 160 mm in the lower part ($h_1 = 4.5$ m high, next to the infills) and 70 mm in the upper, squat part ($h_2 = 1.5$ m high, next to the ribbon windows) of the column. The connection between the new and existing elements is improved by U-shaped steel profiles anchored in the existing element. Implementing the column jacketing also requires (1) removal of the infill sections adjacent to the columns to a width of 50 cm, (2) their replacement after the intervention with the same type of brick, and (3) replacement of the ribbon window along the entire perimeter of the building. The jacketing is combined with UPN300 steel profiles at the main joints between the beams and columns, in accordance with current practice, and with through-holes for ϕ 24 mm steel pins that allow relative rotation while preventing the joints from sliding. The profiles are attached to the columns by eight ϕ 20 mm post-installed fasteners arranged in four rows. The use of spacers is also necessary, especially for a jacketed column, which has an enlarged cross-section. Regarding socket foundations, jacketing of columns requires not only their enlargement but also their strengthening, as the increase in the overall stiffness of the building leads to larger actions at the base of the column. However, this work did not focus on evaluating the seismic safety of the foundation, and it is assumed that the columns are rigidly fixed to the ground.

4.1.2. Building EE2

The retrofit of building EE2 involves a combination of local interventions on (1) the connections between cladding panels and the structure, (2) the connections between the roof and beams, and (3) the columns. The retrofit of the façade panels involves placing four steel brackets (two at the bottom and two slotted at the top) between each horizontal panel and the column (Fig. 6b, d), and two slotted steel brackets between each vertical panel and the beam, as shown in Fig. 6a. The two steel brackets at the bottom of the horizontal cladding panels are designed to support the entire weight of the panels, while the brackets at the top of the panels (vertical and horizontal) counteract panel tilting and accommodate the required in-plane displacements (6.4 cm and 16.0 cm for the horizontal and vertical directions, respectively).

The second local intervention involves preventing the loss of support of the roof elements on the beams by retrofitting the roof-beam connections. New connectors are used, consisting of an L-shaped steel profile with stiffeners, mounted on the front part of the beam and fixed to each roof element (Fig. 6c). The capacity design for each failure mechanism is determined according to building codes: (1) the beam side is designed to prevent bolt failure in tension and plate punching, while (2) the roof element side is designed to prevent bolt failure in shear and bearing. The final geometry of the connection is defined so that its load-bearing capacity is governed by the bearing failure of the roof element

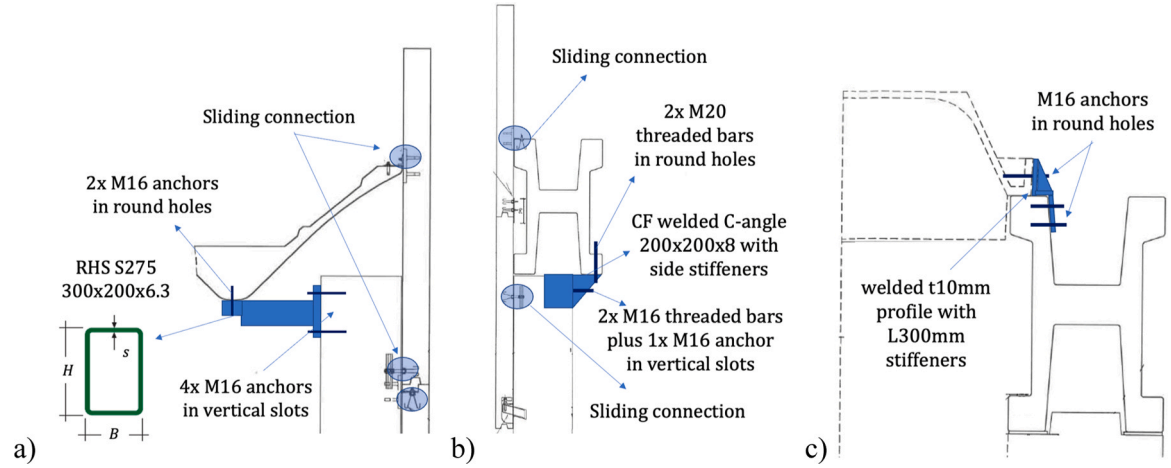

Fig. 8. Building EE4 – retrofit interventions: (a,b) connections of cladding panel and panel-support columns to deck connections, (c) roof-to-beam connections.

connection (with a resistance force of 61.1 kN), allowing ductile failure by milling the steel plate on the roof element side around the bolt hole.

The third and final retrofit measure involves concrete jacketing of the columns (Fig. 6e). Although the deficiency identified in the reference building relates to flexural failure of the column, flexural strengthening can result in shear failure. After flexural strengthening, the safety index for shear strength falls below 1. Therefore, the jacketing extends over the entire height of the column. In addition, technical limitations requiring complete removal of the cladding panels restrict the application of jacketing to all four sides of the columns. Consequently, the three free inner sides are partially sheathed. However, the four corner cladding panels on the façade must be removed and replaced with special corner cladding. In this case, the final layout consists of a 10 cm-thick jacket with a 3 cm concrete cover, ten ϕ 14 mm additional longitudinal reinforcement bars, and ϕ 8 mm stirrups at 20 cm spacing.

4.1.3. Building EE3

The feasibility of various interventions on the main connections between beams and columns is examined. All proposed retrofitting techniques use bolted connections for steel plates and/or angles between the additional device and the structural elements (both column and beam). Among these, the three-hinged arch device, in either its traditional or dissipative configuration [55-57], can effectively reduce the seismic vulnerability of dry connections under horizontal forces. In particular, applying the device in the longitudinal direction of the building (Z-axis) represents a new approach to the system that has not been investigated before. However, premature failure may occur with any solution if the concrete cover for the bolted connections is very small. Therefore, the only possible solution is to insert a single dowel that passes through the beam and is anchored in the column, as shown in Fig. 7a,c for corner and side columns, respectively. The engagement is designed in accordance with NTC 2018 [40,41], considering the low ductility class (CD "B"). According to the code, the horizontal design force is determined as the maximum value between the response spectrum analysis and the plastic shear (corresponding to the maximum flexural capacity), multiplied by the appropriate capacity design coefficient that accounts for overstrength, here $\gamma_{Rd} = 1.2$ for precast reinforced concrete structures with fixed base columns and hinged horizontal elements.

As the Italian code does not specify the shear strength of the anchor, this is assessed using the empirical formulations from CNR 10025/1984 [58], which take into account ductile (global) failure of the dowel connection, i.e. yielding of the dowel and crushing of the surrounding concrete. Steel class 10.9 is selected for the dowels. Although this solution provides a greater concrete cover for the dowel compared to the other techniques investigated, it still results in a brittle failure of the connection. This verification is consistent with the experimental evidence of Vintzeleou and Tassios [59], which shows that ductile failure is the predominant failure mode when the concrete cover exceeds 6–7 times the dowel diameter, while brittle splitting failure is expected at lower concrete covers. The latter scenario occurs for corner columns (1) on the beam side (both X- and Z-axes) and (2) on the column side (X-axis only). This failure mode also occurs for lateral supports on the beam side (Z-axis only).

In these cases, additional measures are taken to restrain the concrete and prevent spalling of the dowel cover, allowing ductile failure to develop. Such interventions include CFRP sheathing and pre-loaded steel plates. To ensure ductile behaviour of the connection until failure, the load-bearing capacity is designed with consideration of the shear strength of the dowel. It is noteworthy that the strength calculations neglect the FRP perforated strips due to the pre-loaded plate anchorage. Fig. 7b, d show the final configuration of the retrofitted connections for the corner and side columns, respectively.

4.1.4. Building EE4

The results of the previously summarised survey clearly indicate that retrofitting interventions should primarily target the panel-to-structure and roof-to-beam connections. Once these vulnerabilities have been addressed through localised strengthening techniques, the columns and beam-to-column connections must also be strengthened to bring the building into full compliance with current seismic codes. It is important to note that retrofitting the column requires actual strengthening rather than merely improving its ductility, as the failure mode in the non-retrofitted configuration is ductile. As an alternative to column jacketing, for building EE4 the installation of dissipative connections is considered to improve the overall performance of the structure by providing additional damping, stiffness, or both. Before this, the effectiveness of dissipative connections [60] and dissipative braces [61] is investigated. Both solutions must be carefully designed, especially considering the absence of a rigid roof diaphragm [61–64]. To design this intervention, the classical response spectrum method based on dynamic elastic modal analysis would not properly account for the nonlinear effect of most energy dissipators. Therefore, a non-linear static method is used, as provided for in NTC 2018 [40,41] and based on the Capacity Spectrum Method (CSM) [65].

The results of the CSM procedure indicate that the columns do not actually require strengthening with such an advanced computational method. This outcome may be explained by the refined calculation approach of the CSM, which accounts for the mechanical and geometrical nonlinearities of the system, including the damping effect caused by the hysteresis of the columns. It should also be noted that the dissipation provided in the CSM remains entirely within the elastic

Table 3
Synoptic table on design of seismic retrofit interventions for the case study buildings.

Building	EE1	EE2	EE3	EE4
Column retrofit	RC jacketing	RC jacketing	*Not used*	*Not used*
Beam-to-column connections	Steel profiles	Bolted steel angles	Dowel bar with steel profiles and FRP sheets	Steel fasteners
Roof-to-beam connections	*Not used*	Steel profiles	*Not used*	Steel fasteners
Panel-to-column connections	*Not used*	Bolted steel angles	*Not used*	Sliding fasteners on panel-support columns and frame columns
Retrofit design method	Response spectrum	Response spectrum	Response spectrum	Capacity spectrum

behaviour range of the columns, as the performance points identified are all below the yielding drift. The measures shown in Fig. 8 are implemented. Metallic sliding connections are added to the existing connections by subsequently installing small-diameter mechanical fasteners [66] to effectively decouple the motion of the panels and the structure [67]. It is assumed that these joints are added to the existing ones without cutting them, at a point very close to the original connection. The issue of lateral vibrations of the independent panel support column is addressed by installing horizontal braces made of H-sections bolted to the tops of the columns along the façade direction, and by connecting the tops of the independent columns to the edge element (either beam or roof, depending on the façade orientation) with steel elements to prevent differential out-of-plane movements. The dowel connections between the roof and beam are strengthened by the post-installation of strong, rigid angle sections bolted together with mechanical fasteners.

4.2. Practical implications of seismic retrofit interventions

Table 3 summarises the main features of each building in terms of building features, assessment of as-built conditions, and design of retrofit interventions. The selection and related design of the proposed retrofit strategies did not merely focus on code compliance for relevant failure modes listed in Table 2. Numerous practical requirements have been considered for the realistic and practical feasibility, including:

- the overall compatibility with typical construction techniques for precast buildings (e.g., structures with monolithic columns and pin-ended beams).
- the use of traditional and widely adopted techniques in current practice in Italy (for example, modern dissipative devices have been excluded).
- the control of direct and indirect costs (e.g. upfront monetary expenses, specialised manpower, and business interruption).
- invasiveness and constructability (e.g., the possibility of dry installation without mortar).
- long-term maintenance and post-event repair (e.g., feasibility of close-up inspections and replacement after damage).

Column RC jacketing in EE1 and EE2 was considered the most efficient solution to comply with the required standards for bending seismic capacity. However, the effectiveness of this approach comes at a high cost, not only in terms of manpower and expenditure, but also in construction time, which is likely to lead to prolonged business interruption due to invasive temporary scaffolding and site operations. Furthermore, the stiffening effect induced by RC jacketing may have a cascading impact on the seismic demand of the foundation system, which may necessitate strengthening that is often impracticable. For these reasons, RC jacketing was not applied in EE4, and code-compliant safety was achieved through connection strengthening and advanced analysis via CSM. Regarding the long-term vulnerability of RC jacketing to ageing and other hazardous events (such as fire) over the structure's lifetime, limited maintenance is typically required except in aggressive environments that may initiate corrosion or other deterioration processes [68]. In the context of life-cycle seismic hazard and mainshock–aftershock sequences, cumulative seismic damage to jacketed columns may not be locally restored, impairing the efficiency and usability of the retrofit system.

Local interventions to beam-to-column, roof-to-beam, and panel-to-structure connections were widely adopted in all buildings to improve diaphragm effects and prevent cladding failure. Mechanical, dissipative, and sliding devices investigated in all buildings can be easily installed with low upfront costs, and operations can be carried out overnight. Interference with ongoing industrial activities is generally minimal, especially for strengthening operations on accessible roofs. Despite the affordability of the adopted local strengthening interventions, the residual seismic risk of the structural assembly may remain significant if they are not combined with interventions aimed at increasing the capacity of the structural members in the main frames. Furthermore, periodic inspections and preventive maintenance to mitigate environmental hazards are strictly required to extend the service life of existing buildings' metallic devices (for all buildings) and FRP sheets (in EE3).

Although beyond the scope of this paper, dissipative retrofit devices merit special mention as the most viable among innovative alternatives to traditional approaches. These devices include friction rotation dampers installed at beam-to-column connections and dissipative

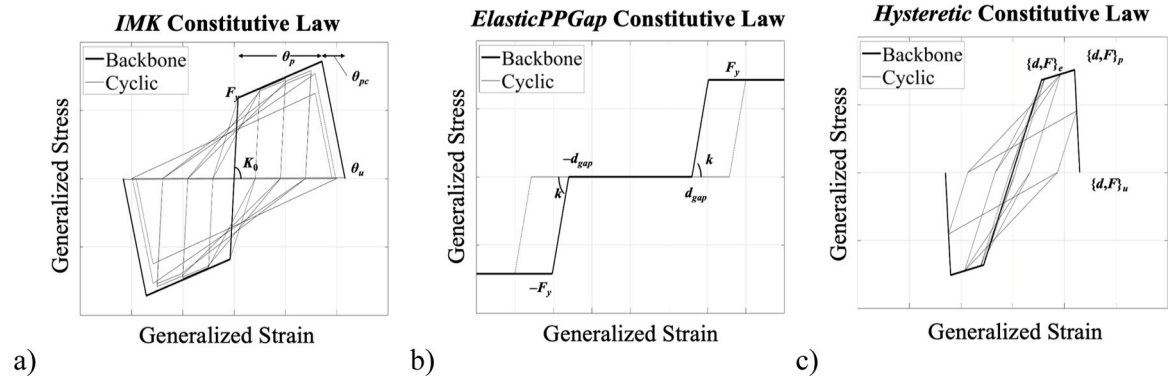

Fig. 9. Relevant parametric hysteretic models for as-is and retrofitted buildings: (a) Modified IMK Deterioration Model with Peak-Oriented Hysteretic Response, (b) Elastic-Perfectly Plastic Gap material, (c) and Hysteretic material.

bracing systems serving as sacrificial elements. Further insight into the combined use of these retrofit strategies for existing industrial buildings can be found in [69]. In addition to improving the global ductility and strength of the building, dissipation-based retrofit strategies have proved to be more sustainable solutions compared to traditional ones. This is due to the localisation of damage within the newly installed dissipative devices, minimising waste production and the consumption of replacement materials [15].

5. Numerical modelling for non-linear structural analysis

This section presents advanced numerical models used for the seismic risk assessment of the investigated buildings, both before and after retrofit interventions. The following subsections outline the modelling assumptions and provide specific details on the incorporation of retrofit interventions into the numerical models.

5.1. General modelling assumptions

For all the buildings investigated, three-dimensional nonlinear numerical models are developed using the OpenSees software [70]. Columns and diaphragm members (i.e., beams and roof elements) are modelled as elastic elements, accounting for their equivalent cross-sections. The columns are assumed to be fixed at the base due to the rigid restraint provided by the socket foundation. The nonlinear response is characterised by a lumped plasticity approach, with a zeroLength element at the column base.

Fig. 9 illustrates the generalised stress-strain relationships adopted in the numerical modelling of the analysed buildings. Envelope curves are shown with thick lines, while hysteretic behaviour is indicated with thin lines. The moment-rotation monotonic backbone and hysteretic response are assigned using the Modified Ibarra-Medina-Krawinkler (IMK) Deterioration Model with Peak-Oriented Hysteretic Response material [71], as presented in Fig. 9a. This also includes the additional plastic hinges introduced in EE1 on the columns at a height of 4.5 m, simulating the flexural behaviour of squat columns adjacent to ribbon windows. The selected OpenSees uniaxial material is characterised by assuming the moment-chord rotation relationship by Fischinger et al. [72], which considers a trilinear backbone with secant-to-yielding initial stiffness, a hardening branch before softening, and zero residual strength. For the monotonic response, evaluations are performed according to the studies by Fardis and Biskinis [73] and Haselton et al. [74], while for the cyclic behaviour, the degradation parameter λ by Ibarra et al. [71] is adopted. This modelling strategy has been widely used for precast RC buildings and validated in the literature [23,25,75]. Diaphragm dowel connections are modelled using equivalent nonlinear zeroLength elements with empirically calibrated IMK force-deformation relationships, where the yield and ultimate strengths of connections are calculated based on mean material resistances in accordance with ISO 20987:2019 [76]. Fig. 9b then shows the bilinear with initial gap (ElasticPPGap) force-deformation model adopted for the retrofit of panel-to-structure and roof-to-beam connections in EE2.

Finally, Fig. 9c shows the constitutive force-deformation hysteretic model of post-installed mechanical fasteners used for retrofitted diaphragm connections in EE4. Additional modelling assumptions for the roof diaphragm, panel cladding, and other elements related to the retrofit interventions are discussed separately for each building. For further details on the as-is building modelling assumptions, see Bosio et al. [31].

5.2. Modelling of retrofit interventions

For the retrofit interventions, advanced modelling techniques are applied to each building to accurately represent the proposed upgrades. For building EE1, the steel profiles designed to allow relative rotations between beams and columns while preventing joint sliding along both principal directions are modelled as cylindrical hinges. Specifically, rotations are restricted around the axis of the main beams up to a certain torsional moment value. To capture this behaviour, a rigid-plastic model is implemented using a multi-linear material with steep initial stiffness and moment capacity derived from a plastic collapse analysis on an equivalent beam cross-section. The new concrete jacket extends to the cross-section core in accordance with current code provisions, as the concrete class is similar to the existing material. This results in improved mechanical properties for both the elastic member and the two plastic hinges, located at the base and at a height of 4.5 m. The latter hinges have different backbone curves, numerically calibrated for the columns, due to varying levels of confinement in the upper and lower squat parts of the column. This is clarified by the mechanical parameters in Table 4, where the two plastic hinges (base and squat column) display identical cyclic behaviour in the original model (first row of the table) and different behaviour in the retrofitted model (second and third rows of the table) [69]. In both Table 4 and the subsequent Table 6, the listed parameters are the elastic stiffness (K_0), yielding moment (M_y), pre-capping rotation (ϑ_p), post-capping rotation (ϑ_{pc}), and ultimate rotation (ϑ_u).

For building EE2, the retrofit interventions on the connections between precast elements are modelled by adding new *zeroLength* elements in parallel to the existing ones to simulate the behaviour of the connections. Column concrete jacketing is incorporated by updating the plastic hinge at the base of the column and the geometric properties based on the new cross-section. The parameters used in the modelling of the new connections and for the jacketed columns are provided in Table 5 and Table 6, respectively. In addition, the exterior cladding is explicitly modelled. For the transverse facades, vertical precast panels are considered, anchored to the ground and connected to the main

Table 4
Building EE1 – plastic hinge parameters of the column.

Model & Element	K_0 [kNm/rad]	M_y [kNm]	ϑ_p [rad]	ϑ_{pc} [rad]	ϑ_u [rad]
As-is Both hinges	1.94E + 04	216.80	0.0204	0.1	0.1316
Retrofitted Base hinges	6.07E + 04	914.54	0.0293	0.1	0.1438
Retrofitted Squat column hinges	6.07E + 04	914.54	0.0620	0.1	0.1764

Table 5
Building EE2 – modelling features of the new connections: gap, elastic stiffness k and yielding strength F_y.

Connection	d_{gap} [m]	k [kN/m]	F_y [kN]
Bottom panel-column	0.000	25,000	36.6
Top panel-column	0.064	36,600	36.6
Panel-beam	0.160	25,000	42.7
Roof element-to-beam	-	2712	61.1

Table 6
Building EE2 – plastic hinge parameters the column. (Note: the yy and zz axes refer to Fig. 6d).

Direction	K_0 [kNm/rad]	M_y [kNm]	ϑ_p [rad]	ϑ_{pc} [rad]	ϑ_u [rad]
As-is Both hinges	4.31E + 04	262.70	0.017	0.043	0.08
Retrofitted (y-y)	3.0E + 04	353.88	0.036	0.054	0.102
Retrofitted (z-z)	2.34E + 04	317.60	0.039	0.060	0.113

Table 7
Building EE4 – backbone curve points for axial and shear force-deformation laws of single fasteners in terms of elastic limit $\{d;F\}_e$, capping point $\{d;F\}_c$ and ultimate point $\{d;F\}_u$.

Direction	d_e [mm]	F_e [kN]	d_c [mm]	F_c [kN]	d_u [m]	F_u [kN]
Axial	1.0	23.0	10.0	70.5	22.0	0.0
Shear	5.6	54.5	12.0	60.5	13.0	0.0

Table 8
Building EE4 – series-parallel arrangements of fasteners in roof-to-beam, beam-to-column, and roof-to-column connections. Clusters are combined in parallel (||) and in series (+) for axial (A) and shear (S) constitutive laws.

Connection	X–axis	Z–axis
Roof-to-beam	(A || A)	(S || S) + (S || S)
Beam-to-column	(S || S || S)	(S || S || S)
Roof-to-column	(S || S) + (S || S)	(S || S) + (A || A)

beams via mechanical devices. In the longitudinal direction, three rows of horizontal panels are provided, connected to the columns via mechanical devices. The upper and lower connections of the precast panels are modelled differently. The lower connection, consisting of a bolt seated in a special seat, supports the panel. The upper connections between the panels and the structure are modelled by inserting several hysteretic models in parallel.

For building EE3, the modelling of the strengthened connections is simplified, as it involves a hinge constraint at the beam-to-column connections to prevent relative displacements between the elements. Non-linear friction elements are replaced by perfect hinge constraints using the *equalDOF* OpenSees command. This simplified approach is supported by the findings of Magliulo et al. [28], who showed that more refined modelling for dowel connections does not improve the accuracy of collapse condition assessments.

Finally, for EE4, the sliding connections are modelled using a pair of *FlatSliderBearing* elements linking the cladding-to-frame assembly. These elements incorporate Coulomb friction ($\mu = 0.22$ based on Dal Lago and Lamperti Tornaghi [66]) and elastic shear springs in the out-of-plane direction with stiffness $k_{shear} = 250$ kN/m. Axial restraints are perfectly rigid, whilst torsional and bending rotations are free. Non-linear springs are applied in parallel with those simulating the behaviour of the existing connections. When the cladding panel connections reach their maximum displacement, the *MinMax* material command simulates the failure of the connection. Afterward, the panels lose two degrees of restraint. If another connection on the same panel reaches its maximum displacement and the *MinMax* material is activated again, the panel collapses due to lack of restraints. Other retrofit solutions involve the installation of stiff metallic brackets between the structural members of the frame structure using post-installed mechanical fasteners. These brackets are assumed to be very stiff, and the deformability of the joint is modelled based on the fasteners only. Non-linear springs are defined in parallel and/or in series based on the configuration of the connections, with non-linear force-displacement laws calibrated from original experimental tests conducted in both axial and shear directions with respect to the diameter 16 mm-fasteners installed in concrete with similar class to the investigated structure. Table 7 shows the constitutive parameters of the force-deformation laws adopted for axial and shear behaviour of a single fastener based on the *Hysteretic* model previously presented in Fig. 9c. Table 8 groups the clusters of shear and axial springs for each roof-to-beam, beam-to--column, and roof-to-column connection along X- and Z-axis. Spring clusters are annotated combining the following operators: parallel (||), series (+), axial (A), shear (S).

6. Performance-based seismic assessment

6.1. Pushover analysis

The first comparison between the original and the retrofitted structures is carried out using non-linear static analyses (pushover) in both principal directions. The results are summarised in Fig. 10 for all four case study buildings in terms of lateral strength ratio (i.e. base shear normalised by the total mass of the roof) versus roof displacement. The main finding from the normalisation is that buildings EE1 and EE3 exhibit maximum lateral strength ratios greater than one, while ratios for EE2 and EE4 remain consistently below one. The primary difference between these buildings is the presence of infill walls. This difference was also evident in the non-normalised version of the pushover curves.

In building EE1 (Fig. 10a), the masonry infills provide high initial stiffness, particularly in the longitudinal direction (Z). In the original, unretrofitted model, non-linearities occur at low lateral displacements due to the formation of plastic hinges. In the transverse direction (X), plastic hinges form at the base of the columns. In both directions, flexural hinges develop in the columns at the location of the ribbon glazing system, a phenomenon commonly known as the “squat column” effect. In the original model, after dowel collapse in the joints, there is also a loss of support in both directions, with the pushover curve becoming flat. In the retrofitted model, the introduction of pinned connections affects the base shear resistance, especially in the longitudinal direction. Concrete jacketing significantly increases not only the shear capacity, but also the initial stiffness and global ductility. In the transverse direction, the formation of plastic hinges is preceded by the failure of the compressed struts in the wall infills.

A different behaviour is observed in Building EE2 (Fig. 10b), where the cladding panels connected to the main elements increase the overall structural stiffness, although their effectiveness is lower than that of masonry infills. The failure of the roof-beam connection is the governing collapse mechanism in the longitudinal direction, while reaching the flexural capacity of the column base determines the global failure mode in the transverse direction. The elastic range extends to the activation of the roof-to-beam mechanical connections once the frictional forces are overcome. The onset of non-linearity corresponds to yielding at the column base. Performance improvements are also significant in terms of displacement ductility (especially along the X-axis) and shear capacity (especially along the Z-axis).

The pushover curves of building EE3 (Fig. 10c) display an initial stiff elastic phase resulting from interaction with the masonry infills, while the non-linearities are governed by friction. Although the original design of the building accounts for seismic actions, the calculated horizontal design forces at the connections are lower than the frictional resistance of the connection. Therefore, mechanical restraints required by the 1970s regulations are unnecessary. Additionally, the rigid roof diaphragm causes simultaneous in-plane sliding of all principal beams in the event of incipient collapse of the beam-to-column connections. In the retrofitted configuration, the slope of the initial stage increases due to the greater shear stiffness of the dowel connections compared to the neoprene pads in the friction-based supports. A sharp increase in lateral load capacity is observed in both directions. All infill walls reach maximum strength at the same displacement demand, after which softening occurs due to the reduction in cladding resistance, down to the residual strength of the bare frame.

Building EE4 (Fig. 10d) exhibits considerable flexibility due to deformable diaphragm effects and significant second-order effects resulting from the slenderness of the columns. In the elastic phase, the frame structure interacts with the external horizontal cladding panels, but this stiffening contribution gradually diminishes as the connection system between the panels and the frame fails sequentially. Depending on the loading direction, the panel connections fail both in-plane and out-of-plane. The connection of the secondary columns supporting the panels to the main frames positively affects the ultimate shear capacity,

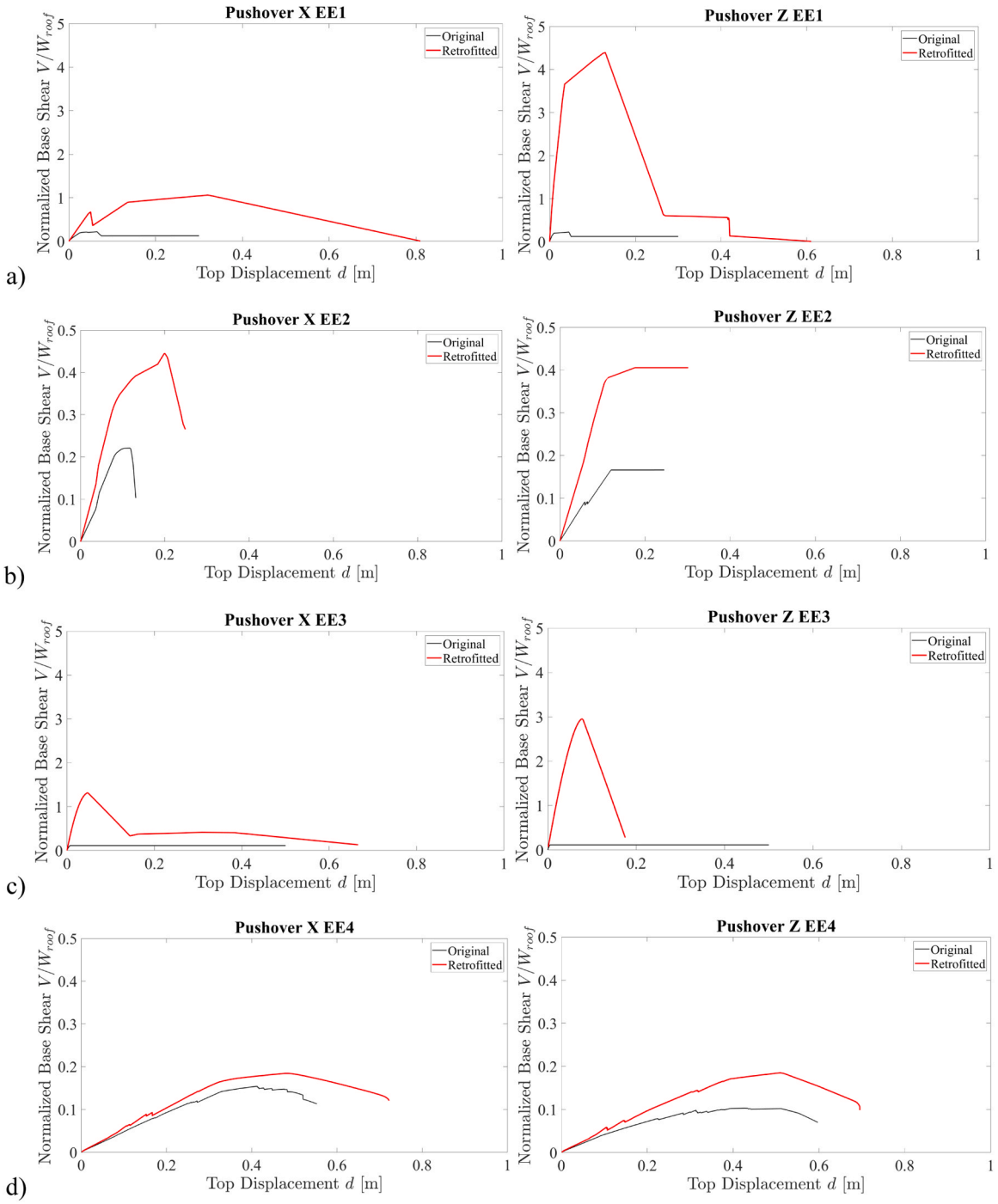

Fig. 10. Normalized pushover response for original building configuration and investigated retrofit strategies, for both horizontal directions. (a) EE1, (b) EE2, (c) EE3, and (d) EE4.

particularly in the longitudinal direction (Z). It prevents out-of-plane collapse of the panels and enables all panel-supporting columns to fully contribute to the building's shear capacity until collapse begins. In both the original and retrofitted configurations, building failure is initiated by the collapse of the dowel connections between the roof and the beams, followed by an immediate loss of support for the roof elements after severe connection damage and concrete spalling. However, retrofitting the roof-to-beam dowel connections enhances both shear strength and ductility, enabling the roof-to-beam connections to withstand increased diaphragm action and better utilise the rotational capacity of the main frame columns.

6.2. *Multi-stripe analysis*

The ground motions and intensity levels were selected in accordance with the RINTC project [68,77], corresponding to the different building typologies considered in the project (i.e. masonry, RC, base-isolated, and steel buildings). Seismic records were selected using a state-of-the-art methodology, consistent with hazard-based spectral shapes and source characteristics in terms of magnitude and distance, based on the conditional spectrum method [78]. The method was further refined to ensure the selected records were consistent with earthquake magnitude and epicentre distance from hazard disaggregation [79]. The records were obtained from the Italian accelerometric archive [80] and,

Table 9
Synoptic table on UPD and GC performance levels in the as-is and retrofitted configurations.

Building	EE1	EE2	EE3	EE4
UPD As-is	0.5 % column drift OR relative joint displacement equal to 10 % of half of the size of the column cross-section	Column yielding rotational capacity OR roof-to-beam connection yielding OR cladding panels collapse	Relative beam-to-column displacement equal to 10 % of the support length	Column-to-panel connection in-plane or out-of-plane failure
UPD Retrofitted	0.5 % column drift	Column yielding rotational capacity OR roof-to-beam connection yielding OR cladding panels collapse	shear base equal to 95 % of the base shear; at least 50 % of the infill panels reaches their maximum strength; at least one infill reaches a 50 % degradation of its maximum strength	Column-to-panel connection in-plane or out-of-plane failure OR sliders peak limit relative displacement
GC As-is	Post-peak 50 % drop in base shear capacity column drift OR Beam support loss	Column ultimate rotational capacity (associated with 50 % strength loss) OR roof-to-beam connection collapse	Beam loss of support	Post-peak 50 % shear capacity column drift OR beam-to-roof dowel limit relative displacement
GC Retrofitted	Post-peak 50 % drop in base shear capacity column drift	Column ultimate rotational capacity (associated with 50 % strength loss) OR roof-to-beam connection collapse	Post-peak 50 % drop in base shear capacity top displacement; Shear failure of the dowel	Post-peak 50 % shear capacity column drift OR beam-to-roof fasteners limit relative displacement

alternatively, from the NGAWest2 database [81]. For the specified site of L'Aquila and for the natural vibration (first mode) period of each building, 200 pairs of record datasets were extracted. Specifically, each record dataset comprises 20 pairs of ground motion signals compatible with 10 reference intensity levels, reflecting different earthquake return periods: [10; 50; 100; 250; 500; 1′000; 2′500; 5′000; 10′000; 100′000] years.

The seismic assessment is carried out using two performance levels: Global Collapse (GC) and Usability Preventing Damage (UPD). Following the multi-criteria approach of Iervolino et al. [69], appropriate Engineering Demand Parameters (EDPs) are selected to characterise the structural performance of both as-is and retrofitted buildings. The performance criteria for GC are based on global deformation capacity, expressed as roof drift ratios corresponding to a specified level of strength degradation for the entire building (i.e., the post-peak drift at 50 % of the shear capacity on the pushover curve). Additional criteria address the occurrence of local failure modes that may compromise the overall stability of the structure under gravity and lateral loads, such as joint failure and beam unseating. The UPD performance criteria concern the onset of either widespread minor damage or severe localised damage that causes significant disruption of use. Conventional limits are also imposed to control global deformation capacity (i.e., roof drift ratio above 0.5 % and total base shear above 95 % of the maximum base shear of the as-is structure).

The variability of the seismic demand for each building is entirely attributed to record-to-record variability of the structural response, with model uncertainties disregarded. Therefore, 20 nonlinear time history analyses were performed using the ground motion suite for each "stripe" associated with an intensity level. Table 9 summarises the conventional failure modes and the EDP threshold values for UPD and GC performance levels adopted for each case study building. The functional meaning of the performance levels for each building is crucial to addressing seismic risk in both as-is and retrofitted buildings. The UPD performance level guarantees immediate occupancy and business continuity without significant damage to non-structural elements. Industrial operations would become untenable due to yielding of diaphragm connections (EE1 and EE3) and column base rotations (EE2), significant stresses on infill walls (EE3), connection failure between cladding panels and main frames (EE2 and EE4), and exceeding conventional limits for roof displacements (EE1). In contrast, the GC performance level denotes exhaustion of the structural system and the onset of kinematic mechanisms threatening life safety. The governing failure mode depends on the main vulnerabilities of each structural typology, including loss of support of beams (EE1 and EE3), ultimate rotational capacity of columns (EE2), ultimate deformation and strength capacity of diaphragm dowels and fasteners (EE2, EE3 and EE4), and conventional limits for roof displacements (EE1).

Fig. 11 shows the Usability Preventing Damage (UPD) and Global Collapse (GC) performance levels. The stacked bar charts represent the observed failure frequency for each performance level, while the demand-to-capacity ratios for all non-failed samples are indicated by dotted markers. Both the bar charts and markers are filled in cyan for UPD and magenta for GC. For each building, two separate graphs are shown for the as-is and retrofitted configurations, on the left and right sides respectively.

It is worth noting that the GC bars are superimposed on the UPD bars, as the damage precedes the collapse. In building EE1 (Fig. 11a), strengthening the beam-to-column connections and jacketing the concrete columns slightly affects the UPD capacity. Conversely, there is a significant improvement in the GC performance level due to the prevention of beam support loss and the considerably greater lateral resistance of the retrofitted model compared to the original building configuration. The reduction in seismic fragility for building EE2 (Fig. 11b) is significant for both the UPD and GC performance levels.

The UPD demand always exceeds the capacity from the 4th stripe in the original configuration, whereas only a small number of analyses indicate UPD failure even at the 10th and final stripe after retrofitting. The amplification also provides a significant benefit to GC performance, as collapse does not occur even at the last stripe. Fig. 11c illustrates the improvement in the seismic performance of the EE3 building, particularly for the UPD limit condition, by increasing the average attainment of UPD capacity from the 3rd to the 6th stripe. It is also shown that the retrofit measures implemented for the GC condition ensure safety for seismic actions with a return period of 475 years, corresponding to a life safety limit state. Finally, the retrofit measures in building EE4 can significantly improve both performance levels investigated by increasing the failure capacity of panel-to-column and beam-to-roof connections. The graphs in Fig. 11d show that the average UPD and GC capacities can be improved from the 3rd to the 6th stripe and from the 5th to the 7th stripe, respectively.

6.3. *Fragility curves and failure rates*

Seismic risk is assessed for both UPD and GC performance levels

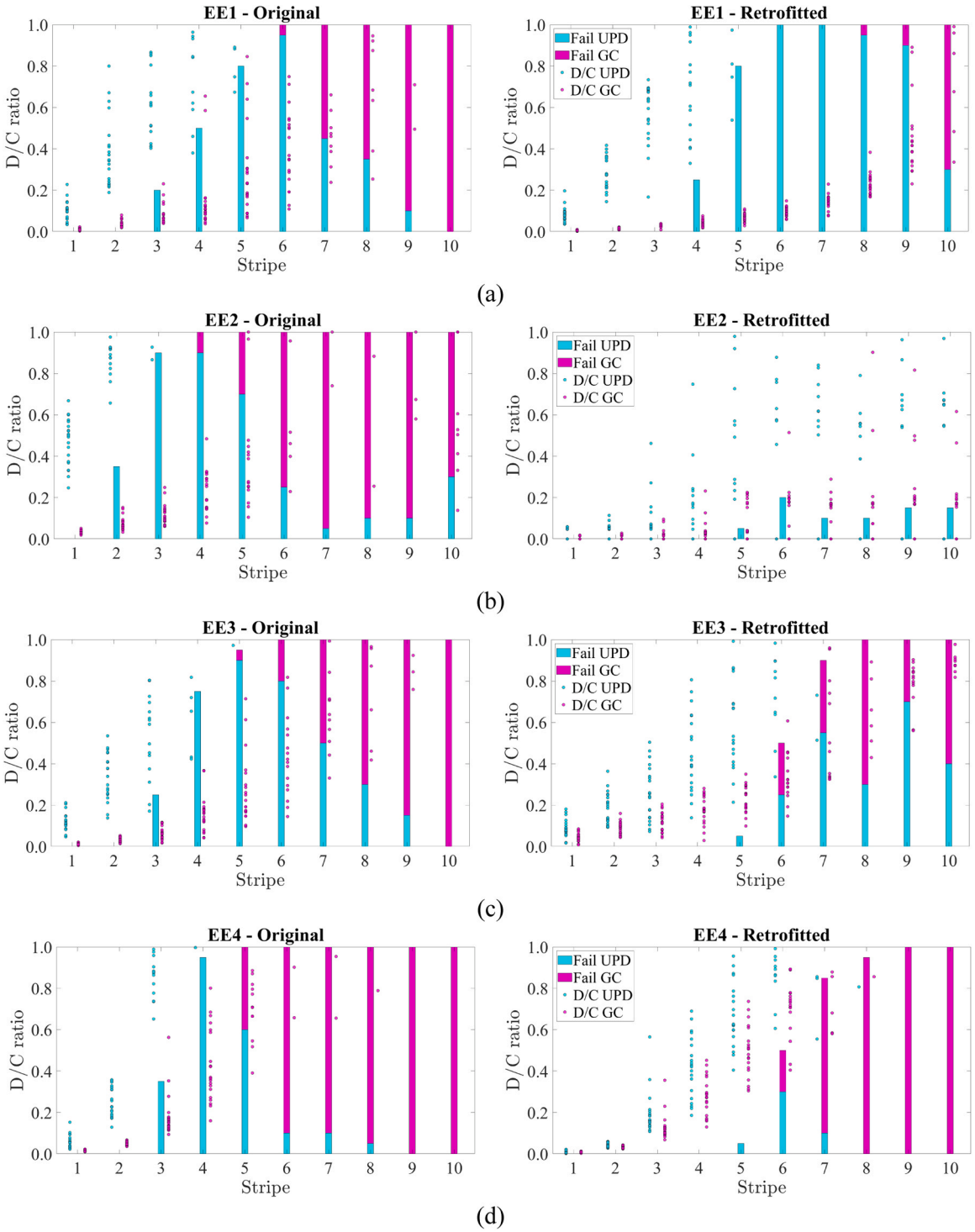

Fig. 11. Results of multi-stripe analysis (MSA) in terms of D/C ratios and failed analyses for UPD and GC performance targets for the as-is and retrofitted configuration. (a) EE1, (b) EE2, (c) EE3, and (d) EE4.

using the R2R-EU software tool, developed within the PBEE paradigm by Baraschino et al. [82]. The tool estimates structure-specific seismic fragility from nonlinear dynamic analyses, quantifies uncertainty due to record-to-record variability, and propagates this to broader risk metrics such as failure rate. To achieve this, R2R-EU applies bootstrap resampling, a statistical method that generates new data sets of equal size by sampling with replacement. Regarding failure rate assessment, low-risk values may be underestimated because the maximum return periods T_R for site-specific hazard curves are limited to 100,000 years [75].

This limitation of the hazard curves to 10^{-5} implies that all failure rate estimates lower than 10^{-5} should be considered unreliable. Therefore, a lower limit of 10^{-5} should be assigned to the failure rate estimates. The Demand/Capacity (D/C) ratios determined by MSA are the engineering demand parameters used to derive the best estimates of the lognormal fragility curves and the mean annual failure rates. The parameters for the lognormal fragility curves and the failure rates are preferably estimated using the maximum likelihood (ML) method [83, 84] with 500 bootstrap extractions to obtain the expected values of the

Table 10
Estimated seismic risk parameters for all case study buildings for UPD and GC performance targets.

Building	Configuration	UPD			GC		
		θ [g]	β	λ [1/yrs]	θ [g]	β	λ [1/yrs]
EE1	Original	0.494	0.399	6.42×10^{-3}	1.977	0.425	5.42×10^{-4}
	Retrofitted	0.612	0.322	3.95×10^{-3}	6.179	0.445	8.11×10^{-5}
EE2	Original	0.043	1.114	4.67×10^{-2}	0.468	1.764	8.98×10^{-3}
	Retrofitted	16.912	1.831	2.80×10^{-4}	-	-	$< 10^{-5}$
EE3	Original	0.409	0.335	8.15×10^{-3}	1.322	0.567	7.51×10^{-4}
	Retrofitted	1.162	0.279	1.18×10^{-3}	2.887	0.887	7.22×10^{-4}
EE4	Original	0.036	0.362	9.64×10^{-3}	0.129	0.457	2.10×10^{-3}
	Retrofitted	0.187	0.372	1.14×10^{-3}	0.227	0.289	7.84×10^{-4}

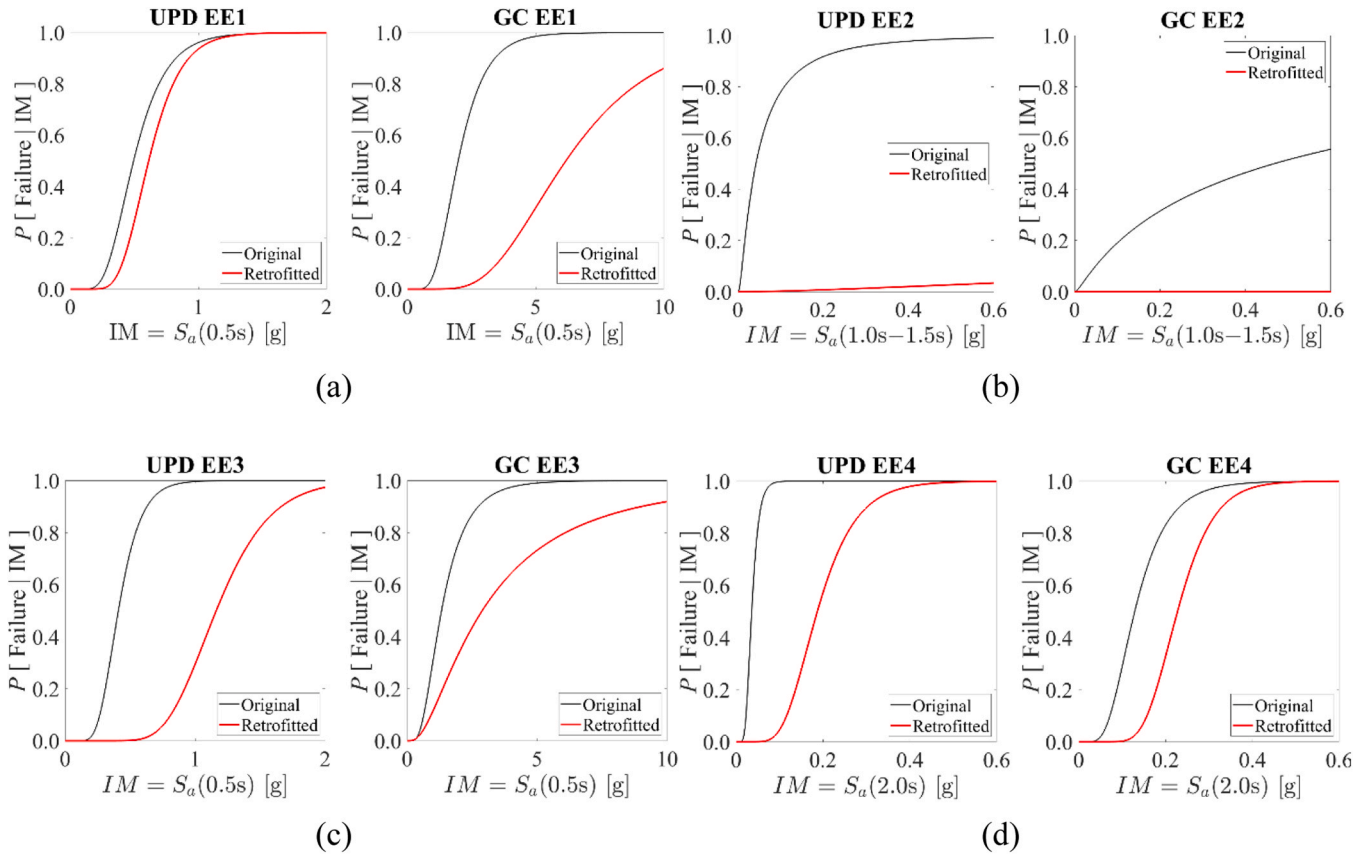

Fig. 12. Fragility curves for UPD and GC performance targets for original building configuration and investigated retrofit strategies. (a) EE1, (b) EE2, (c) EE3, and (d) EE4.

failure rates and fragility parameters.

Collapse due to numerical instability or lack of convergence in the analysis is incorporated into the failure estimation procedure by adjusting the failure frequency at the stripes where such failures occur. Other statistical fitting methods, such as nonlinear least squares regression and the normal probability paper, are also used when convergence issues affect the maximum likelihood method. It is important to emphasise that the fragility curves and failure rates determined for the case study building cannot be easily generalised to other sites. Results may vary due to site-specific hazard characteristics, and different retrofit strategies may be preferable depending on site conditions.

Table 10 presents the numerical values of the following seismic risk parameters: (1) the median seismic capacity θ, (2) the logarithmic standard deviation β, both estimated from the fragility curve fitting procedure, and (3) the mean annual failure rate λ. Fig. 12 and Fig. 13 show the lognormal fragility curves and the mean annual failure rate of exceedance of UPD and GC performance targets, respectively, for all case study buildings in the original configurations and with the retrofit strategies investigated. The reliability of the R2R-EU computational tool is ensured by its validation for probabilistic seismic risk assessment of various structural typologies. In addition, the intensive nonlinear static and dynamic analyses conducted in OpenSees provide robust results in terms of pushover curves and D/C ratios, confirming the effectiveness of the retrofit solutions used. The fragility parameters and failure rate estimates derived from D/C ratios are consistent with the previously obtained results of static analyses.

A key benchmark for quantitatively interpreting the effectiveness of retrofit interventions is provided by the target failure rates implicitly defined by the design procedures regulated by the Italian building code for new buildings. Both UPD and GC implicit failure rates of code-compliant precast RC structures were numerically assessed by Iervolino et al. [22] for multiple sites and soil conditions. Based on simulated design and non-linear seismic analysis of code-compliant archetype structures, the estimated target failure rates for RC structures at the L'Aquila site with soil type C are approximately 6×10^{-3} for UPD and

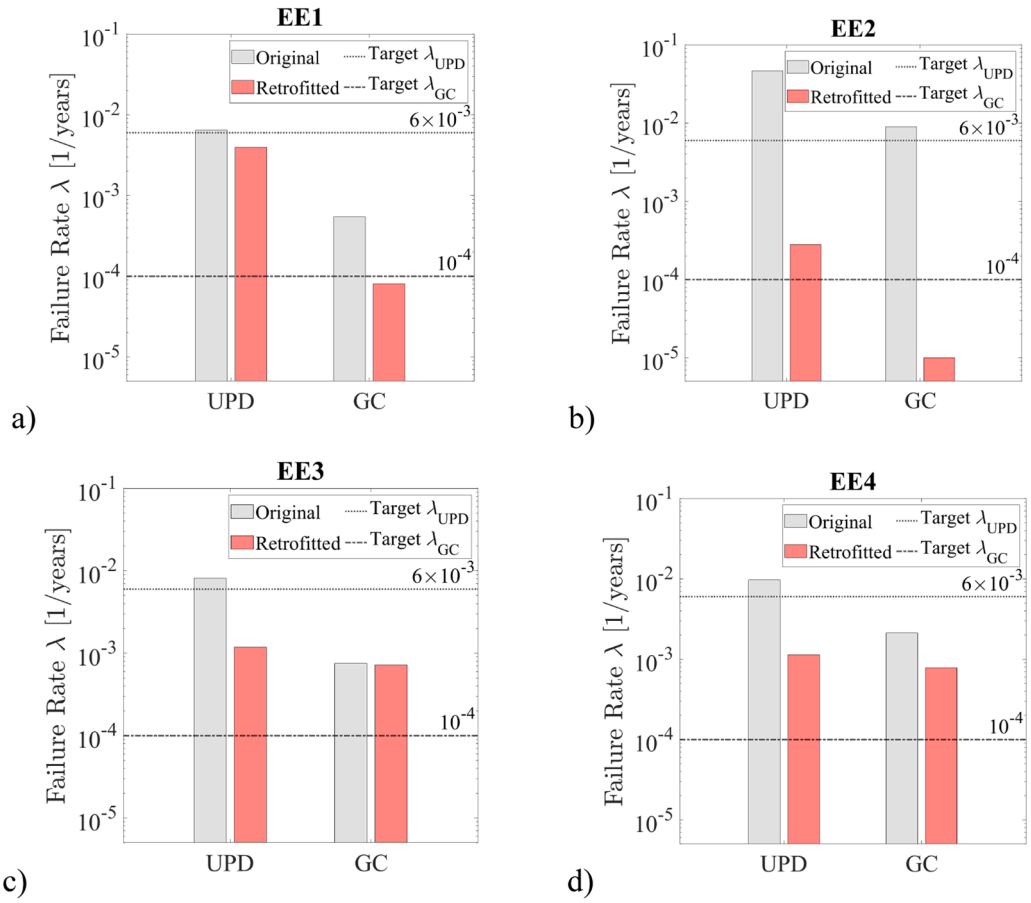

Fig. 13. Mean annual failure rates for UPD and GC performance targets for original building configuration and investigated retrofit strategies. Reference target values at both limit states are also indicated. (a) EE1, (b) EE2, (c) EE3, and (d) EE4.

10^{-4} for GC. The UPD failure rate estimates are below the corresponding target values for all retrofitted buildings, demonstrating that the proposed retrofit strategies can effectively prevent excessive damage that would impair the usability of the industrial facility for the reference hazard level. However, only the buildings retrofitted with invasive interventions such as column jacketing (i.e., EE1 and EE2) show failure rates below the reference GC target.

7. Conclusions

This study examined the impact of various seismic retrofit strategies to enhance the performance of existing precast concrete industrial buildings designed under earlier national codes. Four case studies were analysed, with solutions ranging from local, low-invasive retrofits to global, highly invasive interventions. Depending on each building's vulnerabilities, strategies included strengthening structural connections (beam-to-column, roof-to-beam), improving structural-to-non-structural connections (panel-to-column), increasing column capacity through jacketing, and installing energy dissipation devices. The retrofit solutions considered were developed using code-compliant approaches to simulate current simplified engineering design procedures. The study adopted a Performance-Based Earthquake Engineering (PBEE) framework to quantitatively validate the probabilistic reliability of these code-compliant strategies. The effectiveness of these measures was assessed by analysing the seismic response, deriving fragility curves, and comparing the failure rates of the case-study buildings in both as-is and retrofitted conditions.

The probabilistic assessment highlights a clear distinction in the effectiveness of the investigated retrofit strategies with respect to the Global Collapse (GC) limit state. Highly invasive global strengthening interventions, such as the RC jacketing adopted for EE1 and EE2, are confirmed as the most reliable solutions, achieving the code-implied target failure rate. In contrast, for EE3 and EE4, local, less invasive strategies led to significant reductions in seismic risk but did not meet the same probabilistic threshold. This confirms that code-compliant retrofit measures cannot always guarantee the highest expected reliability against collapse. For the UPD limit state, all interventions were uniformly effective, reducing the annual failure rates below the target values for all archetypes and confirming the positive influence of structural enhancement on the performance of non-structural components. These results highlight the engineering trade-off that inherently exists between safety and practicability: global interventions provide the highest long-term reliability but involve greater costs and construction impact, while local ones offer better feasibility and limited operational disruption at the expense of a higher residual probabilistic risk of collapse. Overall, this dual approach supports the validation of modern codes and provides a crucial data-driven framework for risk-informed decision-making regarding the structural retrofitting of existing precast industrial facilities.

CRediT authorship contribution statement

Chiara Di Salvatore: Writing – review & editing, Visualization, Validation, Software, Methodology, Investigation, Formal analysis, Data curation. **Marius Eteme Minkada:** Writing – review & editing, Visualization, Validation, Software, Methodology, Investigation, Formal analysis, Data curation. **Luca Capacci:** Writing – review & editing, Writing – original draft, Visualization, Validation, Software, Methodology, Investigation, Formal analysis, Data curation. **Paolo Riva:** Writing – review & editing, Validation, Supervision, Project administration,

Methodology, Investigation, Conceptualization. **Andrea Belleri:** Writing – review & editing, Validation, Supervision, Project administration, Methodology, Investigation, Conceptualization. **Davide Bellotti:** Writing – review & editing, Validation, Supervision, Project administration, Methodology, Investigation, Conceptualization. **Francesco Cavalieri:** Writing – review & editing, Visualization, Validation, Software, Methodology, Investigation, Formal analysis, Data curation. **Bruno Dal Lago:** Writing – review & editing, Validation, Supervision, Project administration, Methodology, Investigation, Conceptualization. **Gennaro Magliulo:** Writing – review & editing, Validation, Supervision, Project administration, Methodology, Investigation, Conceptualization.

Funding

The study presented in this article was developed within the activities of the ReLUIS-DPC research program RINTC-implicit seismic risk of code-conforming structures- funded by Presidenza del Consiglio dei Ministri—Dipartimento della Protezione Civile (PCM-DPC). Note that the opinions and conclusions presented by the authors do not necessarily reflect those of the funding entity.

Declaration of competing interest

The authors declare that they have no known competing financial interests or personal relationships that could have appeared to influence the work reported in this paper.

Declaration of Competing Interest

Please find the declaration of Interest Statement of the manuscript entitled “From Code to Performance: Probabilistic Seismic Response of Retrofitted Precast RC Buildings” by Luca Capacci et al.

Acknowledgments

The study presented in this article was developed as part of the activities of the ReLUIS-DPC research program RINTC (implicit seismic risk of code-conforming structures), funded by Presidenza del Consiglio dei Ministri - Dipartimento della Protezione Civile (PCM-DPC). The President of the ReLUIS consortium, Dr. Mauro Dolce, and the coordinator of the project, Prof. Iunio Iervolino, deserve great thanks, as do all the colleagues who participated in the project. The opinions and conclusions expressed here are those of the authors and do not necessarily reflect those of the people acknowledged.

Data availability

Data will be made available on request.

References

[1] Bournas D, Negro P, Taucer F. Performance of industrial buildings during the Emilia earthquakes in Northern Italy and recommendations for their strengthening. Bull Earthq Eng 2013;12(5):2383–404.
[2] Magliulo G, Ercolino M, Petrone C, Coppola O, Manfredi G. Emilia earthquake: the seismic performance of precast RC buildings. Earthq Spectra 2014;30(2):891–912.
[3] Belleri A, Brunesi E, Nascimbene R, Pagani M, Riva P. Seismic performance of precast industrial facilities following major earthquakes in the Italian territory. ASCE J Perform Constr Facil 2015;29(5):04014135.
[4] Savoia M, Buratti N, Vincenzi L. Damage and collapses in industrial precast buildings after the 2012 Emilia earthquake. Eng Struct 2017;137:162–80.
[5] Dal Lago B. Vulnerability assessment of precast industrial facilities. In: Ferreira Tiago Miguel, Rodrigues Hugo, editors. Seismic vulnerability assessment of civil engineering structures at multiple scales: from single buildings to large-scale assessment. Elsevier, Woodhead Publishing; 2021 [ISBN 9780128240717].
[6] Batalha N, Rodrigues H, Sousa R, Varum H. Seismic assessment of existing precast RC industrial buildings in Portugal. Structures 2022;41:777–86.
[7] Labò S, Eteme Minkada M, Marini A, Belleri A. Loss of support assessment for precast portal frames with friction connections and masonry infills. Bull Earthq Eng 2022;20(15):7983–8009.
[8] Cavalieri F, Bellotti D, Nascimbene R. Seismic vulnerability of existing precast buildings with frictional beam-to-column connections, including treatment of epistemic uncertainty. Bull Earthq Eng 2023;21:1117–38.
[9] Bellotti D, Cavalieri F, Nascimbene R. Classification of Italian precast concrete structures. J Build Eng 2025:112787.
[10] Magliulo G, Fabbrocino G, Manfredi G. Seismic assessment of existing precast industrial buildings using static and dynamic nonlinear analyses. Eng Struct 2008;30(9):2580–8.
[11] Belleri A, Torquati M, Riva P, Nascimbene R. Vulnerability assessment and retrofit solutions of precast industrial structures. Earthq Struct 2015;8(3):801–20.
[12] Belleri A, Marini A, Riva P, Nascimbene R. Dissipating and re-centring devices for portal-frame precast structures. Eng Struct 2017;150:736–45.
[13] Javidan MM, Ali A, Kim J. A steel hysteretic damper for seismic design and retrofit of precast portal frames. J Build Eng 2022;57:104958.
[14] Morgen BG, Kurama YC. Seismic response evaluation of posttensioned precast concrete frames with friction dampers. J Struct Eng 2008;134(1):132–45.
[15] Cavalieri F, Bellotti D, Caruso M, Nascimbene R. Comparative evaluation of seismic performance and environmental impact of traditional and dissipation-based retrofitting solutions for precast structures. J Build Eng 2023;79:107918.
[16] Rodrigues H, Batalha N, Furtado A, Arêde A, Sousa R, Varum H. Retrofitting solution for beam-to-column connections of precast reinforced concrete industrial buildings. Eng Struct 2024;302:117424.
[17] Pollini AV, Buratti N, Mazzotti C. Experimental and numerical behaviour of dissipative devices based on carbon-wrapped steel tubes for the retrofitting of existing precast RC structures. Earthq Eng Struct Dyn 2018;47(5):1270–90.
[18] Sorace S, Terenzi G. Existing prefab R/C industrial buildings: seismic assessment and supplemental damping-based retrofit. Soil Dyn Earthq Eng 2017;94:193203.
[19] Guerrero H, Ji T, Escobar JA, Teran-Gilmore A. Effects of buckling-restrained braces on reinforced concrete precast models subjected to shaking table excitation. Eng Struct 2018;163:294–310.
[20] Nastri E, Vergato M, Latour M. Performance evaluation of a seismic retrofitted R.C. precast industrial building. Earthq Struct 2017;12(1):13–21.
[21] Caterino N, Spizzuoco M, Piccolo V, Magliulo G. A semi-active control technique through MR fluid dampers for seismic protection of single-story RC precast buildings. Materials 2022;15(3):759.
[22] Iervolino I, Spillatura A, Bazzurro P. Seismic reliability of code-conforming Italian buildings. J Earthq Eng 2018;22(sup2):5–27.
[23] Ercolino M, Bellotti D, Magliulo G, Nascimbene R. Vulnerability analysis of industrial RC precast buildings designed according to modern seismic codes. Eng Struct 2018;158:67–78.
[24] Magliulo G, Bellotti D, Cimmino M, Nascimbene R. Modeling and seismic response analysis of RC precast Italian code-conforming buildings. J Earthq Eng 2018;22(sup2):140–67.
[25] Cimmino M, Magliulo G, Manfredi G. Seismic collapse assessment of new European single-story RC precast buildings with weak connections. Bull Earthq Eng 2020;18(15):6661–86.
[26] Gajera K, Dal Lago B, Capacci L, Biondini F. Multi-stripe seismic assessment of precast industrial buildings with cladding panels. Front Built Environ 2021;7:631360.
[27] Bressanelli ME, Bellotti D, Belleri A, Cavalieri F, Riva P, Nascimbene R. Influence of modelling assumptions on the seismic risk of industrial precast concrete structures. Front Built Environ 2021;7:629956.
[28] Magliulo G, Di Salvatore C, Ercolino M. Modeling of the beam-to-column dowel connection for a single-story RC precast building. Front Built Environ 2021;7:627546.
[29] Bosio M, Labò S, Riva P, Belleri A. Seismic risk and finite element modelling influence of an existing one-storey precast industrial building. J Earthq Eng 2023;24(1):1363–2469.
[30] Capacci L, Dal Lago B. Structural modelling and probabilistic seismic assessment of existing long-span precast industrial buildings. Bull Earthq Eng 2025;23:2581–609.
[31] Bosio M, Di Salvatore C, Bellotti D, Capacci L, Belleri A, Piccolo V, et al. Modelling and seismic response analysis of non-residential single-storey existing precast buildings in Italy. J Earthq Eng 2023;27(4):1047–68.
[32] De Risi MT, Di Domenico M, Manfredi V, Terrenzi M, Camata G, Mollaioli F, et al. Modelling and seismic response analysis of Italian pre-code and low-code reinforced concrete buildings. Part I: bare frames. J Earthq Eng 2022;27(6):1482–513.
[33] Di Domenico M, De Risi MT, Manfredi V, Terrenzi M, Camata G, Mollaioli F, et al. Modelling and seismic response analysis of Italian pre-code and low-code reinforced concrete buildings. Part II: infilled frames. J Earthq Eng 2022;27(6):1534–64.
[34] Penna A, Rota M, Bracchi S, Angiolilli M, Cattari S, Lagomarsino S. Modelling and seismic response analysis of existing URM structures. Part 1: archetypes of Italian modern buildings. J Earthq Eng 2024;28(4):1130–56.
[35] Lagomarsino S, Cattari S, Angiolilli M, Bracchi S, Rota M, Penna A. Modelling and seismic response analysis of existing URM structures. Part 2: archetypes of Italian historical buildings. J Earthq Eng 2023;27(7):1849–74.
[36] Cardone D, Viggiani LRS, Perrone G, Telesca A, Di Cesare A, Ponzo FC, et al. Modelling and seismic response analysis of existing Italian residential RC buildings retrofitted by seismic isolation. J Earthq Eng 2023;27(4):1069–93.
[37] Franchin P, Baltzopoulos G, Biondini F, Callisto L, Capacci L, Carbonari S, et al. Seismic reliability of Italian code conforming bridges. Earthq Eng Struct Dyn 2023;52(14):4442–65.

[38] Cantisani G, Della Corte G. Modelling and seismic response analysis of non-residential existing steel buildings in Italy. J Earthq Eng 2023;27(3):623–55.
[39] Angiolilli M, Eteme Minkada M, Di Domenico M, Cattari S, Belleri A, Verderame GM. Comparing the observed and numerically simulated seismic damage: a unified procedure for unreinforced masonry and reinforced concrete buildings. J Earthq Eng 2024;28(4):1157–93.
[40] Ministero delle Infrastrutture e dei Trasporti. Norme Tecniche per le Costruzioni-NTC: Gazzetta Ufficiale n. 42 del 20 febbraio 2018. Rome, Italy; 2018. [(in Italian)].
[41] Ministero delle Infrastrutture e dei Trasporti. Circolare 21 gennaio 2019, n. 7C.S. LL.PP. - Istruzioni per l'applicazione dell'Aggiornamento delle "Norme Tecniche per le Costruzioni di cui al decreto ministeriale 17 gennaio 2018, Vol. Gazzetta Ufficiale n. 35 del 11 febbraio 2019. Rome, Italy; 2019. [(in Italian)].
[42] EN 1998-1:2004. Eurocode 8 – design of structures for earthquake resistance Part 1: general rules, seismic actions and rules for buildings; 2004.
[43] Dal Lago B. Experimental and numerical assessment of the service behaviour of an innovative long-span precast roof element. Int J Concr Struct Mater 2017;11(2):261–73.
[44] CNR – UNI 10012-67. Ipotesi di carico sulle costruzioni. Bollettino Ufficiale del CNR, seconda edizione. luglio; 1967. [(in Italian)].
[45] Decreto Ministeriale 30/05/1974. Norme tecniche per la esecuzione delle opere in cemento armato normale e precompresso e per le strutture metalliche. In Suppl. ord. alla G.U. n. 198 del 29/07/1974. [(in Italian)].
[46] Decreto Ministeriale 03/03/1975. Approvazione delle norme tecniche per le costruzioni in zone sismiche. In Suppl. ord. alla G.U. n. 93 del 08/04/1975. [(in Italian)]
[47] Decreto Ministeriale 19/06/1984. Norme tecniche per le costruzioni in zona sismica. G.U. n. 208 del 30/07/1984. [(in Italian)]
[48] G+D Computing. Using Strand7 (Straus7) – introduction to the Strand7 finite element analysis system system. Ed. 3. Sidney, Australia: Strand7 Pty Limited; 2010.
[49] Decreto Ministeriale 09/01/1996. Norme tecniche per il calcolo, l'esecuzione ed il collaudo delle strutture in cemento armato normale e precompresso e per le strutture metalliche. G.U. n. 29 del 05/02/1996. [(in Italian)]
[50] Bonfanti C., Carabellese A., Toniolo G. Strutture prefabricate: catalogo delle tipologie esistenti, s.l.: Reluis, ASSOBETON; 2008.
[51] Midas Information Technology Co. Ltd. Midas Gen v2.1. Integrated solution system for building and general structures; 2022. Website: ⟨https://www.midasuser.com/en/gate/building/⟩.
[52] Computer & Structures Inc. SAP2000 advanced 9.0.3, structural analysis program. Berkeley, California: CSI Computer & Structures; 1994.
[53] Magliulo G, Capozzi V, Fabbrocino G, Manfredi G. Neoprene–concrete friction relationships for seismic assessment of existing precast buildings. Eng Struct 2011;33(2):532–8.
[54] Decanini L., Mollaioli F., Mura A., Saragoni R. Seismic performance of masonry infilled R/C frames. In: Proceedings of the 13th world conference on earthquake engineering (13WCEE). Vancouver, British Columbia, Canada; 2004.
[55] Toniolo G, Dal Lago B. Conceptual design and full-scale experimentation of cladding panel connection systems of precast buildings. Earthq Eng Struct Dyn 2017;46(14):2565–86.
[56] Magliulo G, Cimmino M, Ercolino M, Manfredi G. Cyclic shear tests on RC precast beam-to-column connections retrofitted with a three-hinged steel device. Bull Earthq Eng 2017;15(9):3797–817.
[57] Cavalieri F, Bellotti D, Nascimbene R. Design and modelling of traditional and dissipative techniques for seismic rehabilitation of precast industrial buildings. Bull Earthq Eng 2025;23:6437–64. https://doi.org/10.1007/s10518-025-02285-9.
[58] CNR10025/84. Istruzioni per il progetto, l'esecuzione ed il controllo delle strutture prefabricate in conglomerato cementizio e per le strutture costruite con sistemi industrializzati, vol 107. Bollettino Ufficiale del CNR; 1985. [(in Italian)].
[59] Di Salvatore C, Magliulo G, Caterino N. Innovative hysteretic device for seismic retrofit of single-story RC precast buildings. Eng Struct 2024;313:118261.
[60] Vintzeleou EN, Tassios TP. Mathematical-models for dowel action under monotonic and cyclic conditions. Mag Concr Res 1986;38(134):13–22.
[61] Dal Lago B, Biondini F, Toniolo G. Seismic performance of precast concrete structures with energy dissipating cladding panel connection systems. Struct Concr 2018;19:1908–26.
[62] Dal Lago B, Naveed M, Lamperti Tornaghi M. Tension-only ideal dissipative bracing for the seismic retrofit of precast industrial buildings. Bull Earthq Eng 2021;19:4503–32.
[63] Dal Lago B, Ferrara L. Efficacy of roof-to-beam mechanical connections on the diaphragm behaviour of precast decks with spaced roof elements. Eng Struct 2018;176:681–96.
[64] Dal Lago B, Bianchi S, Biondini F. Diaphragm effectiveness of precast concrete structures with cladding panels under seismic action. Bull Earthq Eng 2019;17(1):473–95.
[65] Ostetto L, Sousa R, Fernandes P, Rodrigues H. Influence and effectiveness of horizontal diaphragms and cladding wall panels on the seismic behaviour of precast RC industrial buildings. Eng Struct 2023;285:116046.
[66] Dal Lago B, Molina FJ. Assessment of a capacity spectrum design approach against cyclic and seismic experiments on full-scale precast RC structures. Earthq Eng Struct Dyn 2018;47(7):1591–609.
[67] Dal Lago B, Lamperti Tornaghi M. Sliding channel cladding connections for precast structures subjected to earthquake action. Bull Earthq Eng 2018;16(11):5621–46.
[68] Iervolino I, Baraschino R, Belleri A, Cardone D, Della Corte G, Franchin P, et al. Seismic fragility of Italian code-conforming buildings by multi-stripe dynamic analysis of three-dimensional structural models. J Earthq Eng 2023;27(15):4415–48.
[69] Iervolino I. Estimation uncertainty for some common seismic fragility curve fitting methods. Soil Dyn Earthq Eng 2022;152:107068.
[70] Bellotti D, Cavalieri F, Nascimbene R. Influence of closure external panels modelling on the seismic response of non-residential precast buildings. J Earthq Eng 2024;28(1):288–304.
[71] McKenna F, Fenves GL, Scott MH. OpenSees: open system for earthquake engineering simulation. Berkeley, CA, USA: University of California; 2000 [Available online: ⟨http://opensees.berkeley.edu⟩].
[72] Ibarra LF, Medina RA, Krawinkler H. Hysteretic models that incorporate strength and stiffness deterioration. Earthq Eng Struct Dyn 2005;34(12):1489–511.
[73] Fischinger M, Kramar M, Isokovi MT. Cyclic response of slender RC columns typical of precast industrial buildings. Bull Earthq Eng 2008;6:519–34.
[74] Fardis MN, Biskins DE. Deformation capacity of RC members, as controlled by flexure or shear. In: Kabeyasawa T, Shiohara H, editors. Performance-based engineering for earthquake resistant reinforced concrete structures: a volume honoring Shunsuke Otani. University of Tokyo; 2003.
[75] Haselton C.B., Liel A.B., Taylor Lange S., Deierlein, G.G. Beam-column element model calibrated for predicting flexural response leading to global collapse of RC frame buildings [PEERRep. 2007/03]. Berkeley, CA: PEER Center, Univ. of California; 2008.
[76] Kramar M, Isaković T, Fischinger M. Seismic collapse risk of precast industrial buildings with strong connections. Earthq Eng Struct Dyn 2010;39(8):847–68.
[77] ISO 20987:2019. Simplified design for mechanical connections between precast concrete structural elements in buildings. Geneva, Switzerland: International Standard Association; 2019.
[78] Spillatura A., Kohrangi M., Bazzurro P., Vamvatsikos D. Conditional spectrum record selection faithful to causative earthquake parameter distributions. Earthq Eng Struct Dyn. Vol. 50(no. 10). p. 2653–71.
[79] Lin T, Haselton CB, Baker JW. Conditional spectrum-based ground-motion selection. Part I: hazard consistency for risk-based assessments. Earthq Eng Struct Dyn 2013;42:1847–65.
[80] Luzi L, Hailemikael S, Bindi D, Pacor F, Mele F, Sabetta F. ITACA (ITalian ACcelerometric Archive): a web portal for the dissemination of Italian strong-motion data. Seismol Res Lett 2008;79:716–22.
[81] Ancheta TD, Darragh RB, Stewart JP, Seyhan E, Silva WJ, Chiou BSJ, et al. NGA-West2 database. Earthq Spectra 2014;30:989–1005.
[82] Baraschino R, Baltzopoulos G, Iervolino I. R2R-EU: software for fragility fitting and evaluation of estimation uncertainty in seismic risk analysis. Soil Dyn Earthq Eng 2020;132:106093.
[83] Iervolino I, Baraschino R, Spillatura A. Evolution of seismic reliability of code-conforming Italian buildings. J Earthq Eng 2023;27(7):1740–68.
[84] Baker JW. Efficient analytical fragility function fitting using dynamic structural analysis. Earthq Spectra 2015;31(1):579–99.